INFORMATION TO USERS

This reproduction was made from a copy of a document sent to us for microfilming. While the most advanced technology has been used to photograph and reproduce this document, the quality of the reproduction is heavily dependent upon the quality of the material submitted.

The following explanation of techniques is provided to help clarify markings or notations which may appear on this reproduction.

1. The sign or "target" for pages apparently lacking from the document photographed is "Missing Page(s)". If it was possible to obtain the missing page(s) or section, they are spliced into the film along with adjacent pages. This may have necessitated cutting through an image and duplicating adjacent pages to assure complete continuity.

2. When an image on the film is obliterated with a round black mark, it is an indication of either blurred copy because of movement during exposure, duplicate copy, or copyrighted materials that should not have been filmed. For blurred pages, a good image of the page can be found in the adjacent frame. If copyrighted materials were deleted, a target note will appear listing the pages in the adjacent frame.

3. When a map, drawing or chart, etc., is part of the material being photographed, a definite method of "sectioning" the material has been followed. It is customary to begin filming at the upper left hand corner of a large sheet and to continue from left to right in equal sections with small overlaps. If necessary, sectioning is continued again—beginning below the first row and continuing on until complete.

4. For illustrations that cannot be satisfactorily reproduced by xerographic means, photographic prints can be purchased at additional cost and inserted into your xerographic copy. These prints are available upon request from the Dissertations Customer Services Department.

5. Some pages in any document may have indistinct print. In all cases the best available copy has been filmed.

University Microfilms International
300 N. Zeeb Road
Ann Arbor, MI 48106

Onady, Gary Michael

PRELIMINARY STUDIES OF A METALLOPROTEIN MODEL SYSTEM

City University of New York PH.D. 1982

PRELIMINARY STUDIES OF A METALLOPROTEIN MODEL SYSTEM

by

GARY M. ONADY

A dissertation submitted to the Graduate Faculty in Chemistry in partial fulfillment of the requirements for the degree of Doctor of Philosophy, The City University of New York.

1982

This manuscript has been read and accepted for the Graduate Faculty in Chemistry in satisfaction of the dissertation requirement for the degree of Doctor of Philosophy.

3/1/82
date

Chairman of Examining Committee

1st March 1982
date

Executive Officer

Supervisory Committee

The City University of New York

Abstract

PRELIMINARY STUDIES OF A METALLOPROTEIN MODEL SYSTEM

by

GARY M. ONADY

Adviser: Dr. David K. Lavallee

Important oxidation-reduction reactions in living systems involve a series of metalloproteins which undergo electron transfer in a highly specific manner. Prosthetic group alignment with the formation of an electron transfer complex is thought to be crucial in determining electron transfer between such proteins. The distances separating prosthetic groups are therefore expected to play an important role in such electron transfer processes.

Two kinetic theories may apply to such systems: the adiabatic Marcus theory, or the nonadiabatic Hopfield theory. Both theories show distance dependence on electron transfer rates. Marcus theory, applied to systems having fixed geometry, predicts an increase in rate with separation of redox centers of the same sign of charge due to favorable electrostatic effects on the outer-sphere activation energy. Hopfield theory predicts an opposite effect for distance dependence on electron transfer rates due to decreased value of the overlap integral between the two wave functions of the redox centers.

The purpose of this project is to investigate electron transfer properties of systems where redox centers are separated by known distances. Androstane and cholestane derivatives were used to separate Ru^{2+} and Co^{3+} reaction centers. Complexes investigated were $[(pic)(NH_3)_4Ru(3,7dac)Co(NH_3)_4(H_2O)]^{5+}$ and $[(pic)(NH_3)_4 Ru(3,7daa)Co(NH_3)_4(H_2O)]^{5+}$ in which metal centers are separated by 7.47 and 13.36 A respectively. Electron transfer rates were observed as identical for both cases with $k = 1.4 \times 10^{-4}\ s^{-1}$. Activation parameters are nearly identical where $\Delta H^{\ddagger} = 22$ kcal/mole and $\Delta S^{\ddagger} = -5$ cal/mole K. Further experiments will be necessary to verify the mechanism of electron transfer observed in the androstane and cholestane derivatives.

PREFACE

There are many people and circumstances which have contributed to my development as a scientist and as a person. For my scientific development, I was most fortunate to have the faculty and undergraduate chemistry curriculum at the University of Cincinnati as an extremely firm foundation to build on. It was Dr. Edward Deutsch who nurtured my research interests, leading to an excellent graduate experience. Chosing Dr. David K. Lavallee as my research adviser was a natural transition. Through Dr. Lavallee, I learned valuable methods of approaching scientific problems in many ways and in many area. He has truly given me confidence in myself as a scientist.

Of course a big part of my graduate education has been my coworkers. I thank all of them for their advice and friendship. In particular, I would like to thank Alan Kopelove for all he has done for me in both the lab and on the cliffs in New Paltz. Those weekend excursions with Alan helped clear my mind for the fresh new week of chemistry which followed. I would like to also thank Berta Anderes whos kissetos helped fog my mind with thoughts other than chemistry which was initially cleared by mountain climbing in New Paltz. A special thanks goes to Dr. S. Jeganathen for his contribution to this project in organic synthesis, and his explanations of the social roles of women in Indian society.

Of the things that kept me going through more difficult times, three stand out as most important to me. The first is my music. My graduate career not only has given me a diverse chemistry experience, but has led also to a wide musical experience; from playing with the C.S.U. Statesmen, to some excellent individuals in both Colorado and in New York City. Music has always been there to help regain control of

my self and my thoughts.

I especially want to take this chance to thank Jon Doi for choosing me as a close friend as well as a coworker. His help in the laboratory was invaluable to my work through his keen knowledge and precise logic. His friendship means even more. The advice he gives somehow always makes sense, and his compassion always shines through, Both he and his wife Debbie, (and of course Stephanie) I consider as my second family.

This brings me to my family. I never really know how to show my appreciation for all my parants and my brother have done for me. Some of the ways of giving to them what they have given to me are in my accomplishments. I could have never achieved what I have without them. My family is my life. I dedicate this work to them.

Finally, I would like to end this preface with an excerpt from Hugh Prather's "Notes to Myself: My Struggle to Become a Person", which summarizes fairly well my graduate research experience:

> I don't live in a laboratory: I have no way of knowing what results my actions will have. To live my life for results would be to sentence myself to continuous frustration and to hang over my head the threat that death may at any moment make my having lived a waste. My only sure reward is in my actions and not from them. The quality of my reward is in the depth of my response, the centralness of the part of me I act from.
>
> Because the results are unpredictable, no effort of mine is doomed to failure. And even a failure will not take the form I imagine. The most realistic attitude for me to have toward future consequences is "it will be interesting to see what happens." Excitement, dejection and boredom assume a knowledge of results that I cannot have.

Thank you, Jenny Gruder, for enlightening me with this phrase, as well as your own thoughts.

LIST OF ABBREVIATIONS

CDCA	chenodeoxycholic acid
daa	diamineoandrostane
dac	diaminocholestane
kha	ketohydroxycholestane or androstanolone
dka	diketoandrostane
dkc	diketocholestane
LAH	lithium aluminium hydride
MES	morpholineethanesulfonic acid
NapTs	sodium tosylate
pacm	bis(paraaminocyclohexyl)methane or 4,4-diaminodicyclohexylmethane
pic	γ-picoline
THF	tetrahydrofuran
UDCA	ursodeoxycholic acid

TABLE OF CONTENTS

LIST OF TABLES

LIST OF FIGURES

CHAPTER 1

INTRODUCTION

A. Discussion of Biological Electron Transfer Proteins

As an increasing number of structures for electron carriers in biological systems are solved, increasing insight into mechanisms of electron transfer is being obtained. The question of the distances over which electron transfer centers interact in the formation of protein-electron transfer complexes however, still remains. As F.R. Salemme most appropriately states:

> "... for the majority (but not all) of known electron transport protein structures, the reactive prosthetic group is disposed to allow more or less direct interaction with the external environment. This would suggest that, in most cases, these molecules react by mechanisms involving interactions between the prosthetic groups in the transition state. However, it is by no means clear whether these intimate interactions are sufficient to allow electron transfer to take place by classical outersphere reaction mechanisms which require direct orbital overlap of the reaction species or are better described as shortrange tunneling processes."[1]

This statement addresses the concern of this thesis: the design of an experimental system to define known distances of electron transfer centers, and investigate electron transfer kinetics. The results will be compared with prediction of the Marcus theory of outersphere electron transfer,[2] and the tunneling theory described by Hopfield.[3] Discussion of both theories will follow, but first a review of several proteins will introduce the thesis.

As biological systems evolved, becoming more complex, so did their demand for the energy to sustain the requirements of an organisms' survival. Evolving with these organisms was a series of electron transfer proteins. The energy yielded by the transfer of electrons down

a potential gradient created by these distinct proteins was coupled to provide energy which could be utilized by the organism - as the phosphate bond in adenosine triphosphate (ATP). Figure 1 illustrates three such systems found in the biosphere, ranging from the more simplistic, cyclic photophosphorylation found in bacteria, to the more complex systems found in the mitochondria of eukaryotes and the chloroplasts of plants. This illustrates one of the many physiological functions electron transfer proteins serve. Even though these systems differ in their complexity and numbers of proteins, they all seem to have the same basic attributes - the electron carriers show exceptional specificity for formation of a particular protein-electron transfer complex.

Two types of structurally known electron transfer proteins, the non-heme ferredoxins and the heme-containing cytochromes, are illustrated in Figure 2. The prosthetic group environment of these proteins has been carefully considered. A consistent feature of these molecules are the metals' fixed-ligand environments, whether it be for enzyme integrity, redox potential, positioning for optimal electron transfer, or any combination of these possibilities. Contrary to catalytically active enzymes, where enzyme-substrate interactions serve to distort the substrate towards the transition state, the electron transfer proteins seem to be best thought of as an integrated whole, with the metal center having little flexibility.

The actual distances between the prosthetic groups of interacting electron transfer proteins in biological systems proposed to date vary from 8-40 Å. James Chien has shown good correlation to Hopfield theory

Figure 1. Electron Transfer Systems Found in the Biosphere.

I. Bacterial cyclic photophosphorylation.

II. Mitochondrial electron transport chain.

III. Photosynthetic electron transport.

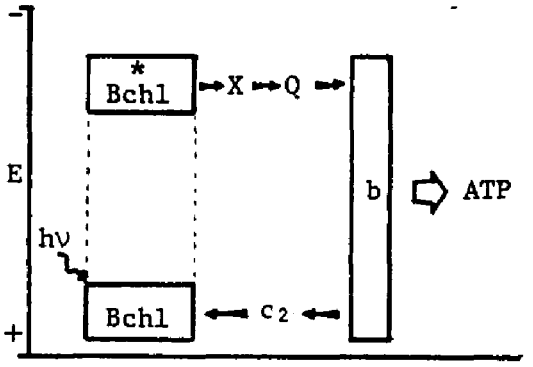
E
-
+
*
Bchl
X
Q
b
ATP
hν
Bchl
c2

I

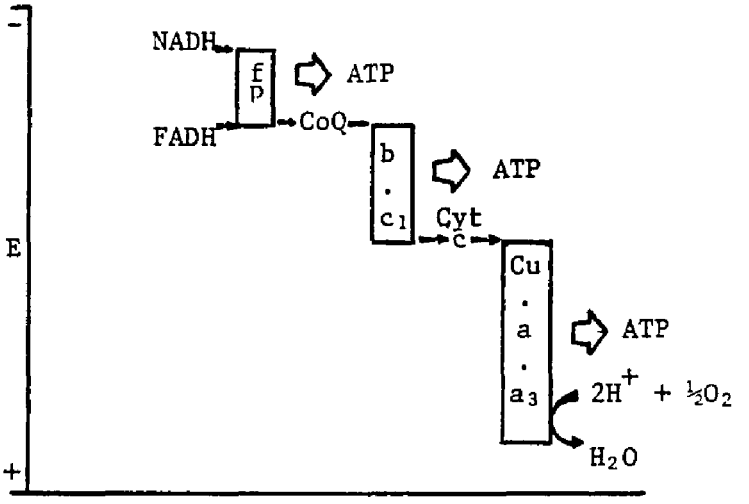
E
-
+
NADH
FADH
f
p
ATP
CoQ
b
·
c1
ATP
Cyt
c
Cu
·
a
·
a3
ATP
2H+ + ½O2
H2O

II

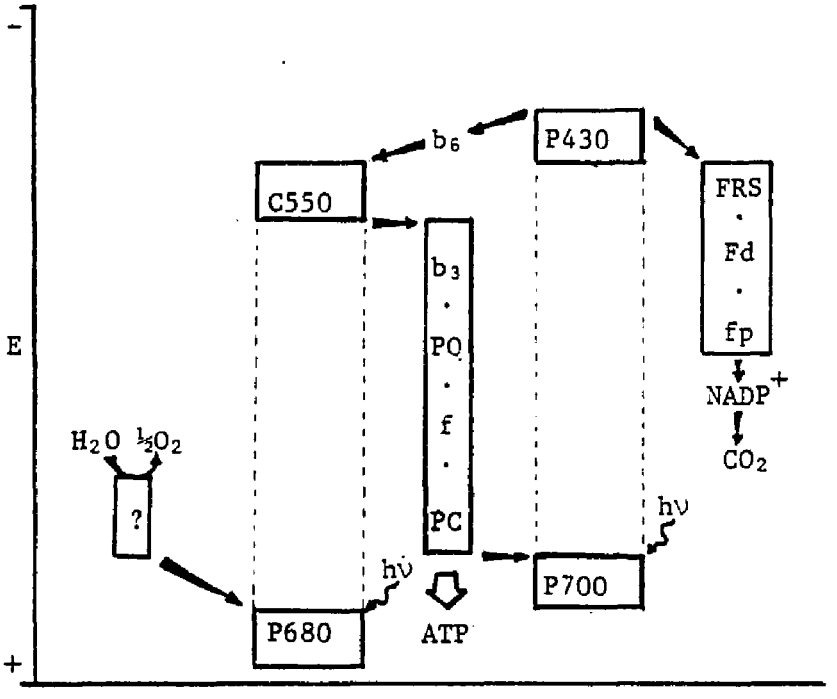
E
-
+
b6
P430
C550
FRS
·
Fd
·
fp
b3
·
PQ
·
f
·
PC
NADP+
CO2
H2O ½O2
?
hν
hν
P680
ATP
P700

III

Figure 2. Ribbon Backbone Representations of Various Electron Transfer Proteins.[1]

Non Heme Iron Proteins - The darkened atom is iron.

I. Rubredoxin - Iron bound to protein by four cysteine residues.

II. Ferredoxin - Iron bound to protein by one cysteine residue, while coordinated in the three remaining positions by inorganic sulfur.

III. High Potential Iron Protein - Iron bound similarly as in Ferredoxin.

Heme Containing Cytochromes.

IV. Cytochrome c - Dotted structure is deleted in the smaller cytochromes.

V. Cytochrome b - Unlike the c cytochromes, the porphyrin is not covalently linked to the protein.

I.

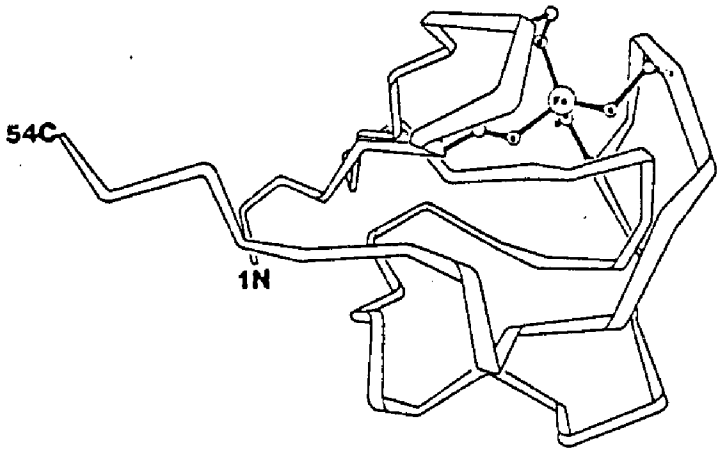

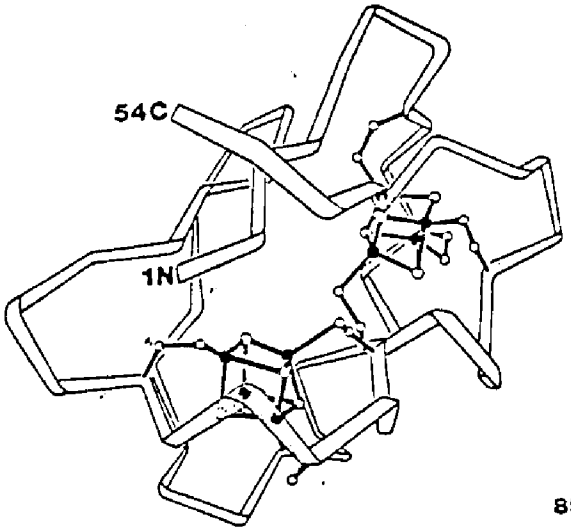

II.

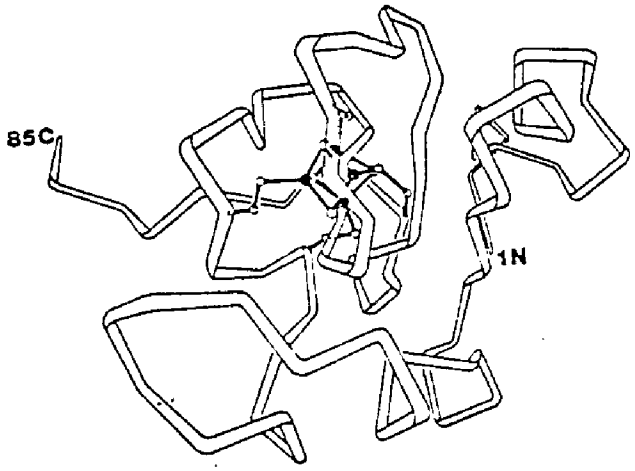

III.

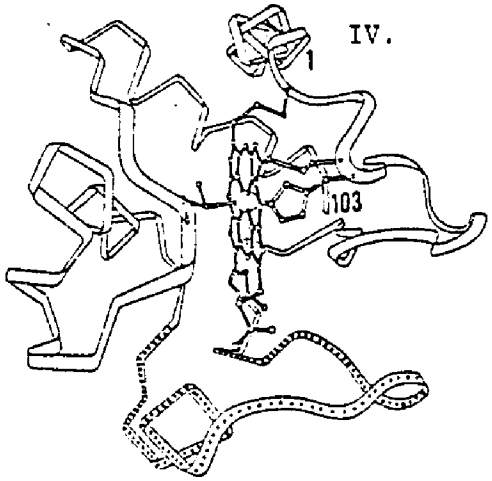

IV.

V.

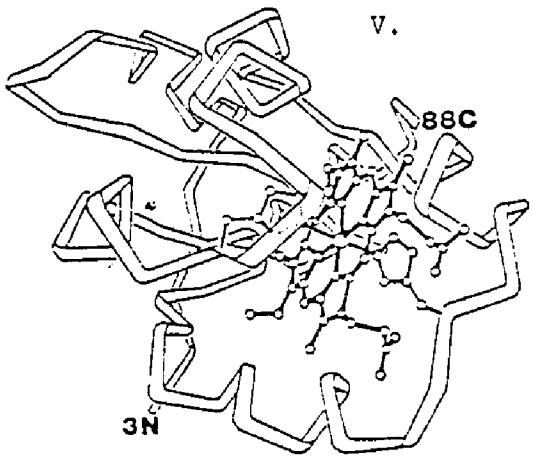

prediction of electron tunneling with a series of cytochrome c metal derivatives, where he estimates the distance of interaction to be 4 Å.[4] Jane Vanderkooi, et.al.,[5,6] performed a fluorescence experiment applying Forster theory to tin derivatives of cytochrome c to study the distances predicted in the cytochrome c-cytochrome oxidase redox pair. The results were based on the distance relationship:

$$R_o^6 = 8.785 \times 10^{-25} \kappa^2 \Phi n^{-4} \int_0^\infty e(\lambda) f(\lambda) d\lambda \qquad (1)$$

in which R_o is defined as the distance at which a fluorescent donor is 50% quenched by an acceptor with Φ being the emission quantum yield of the donor in absence of the acceptor, n the refractive index, $e(\lambda)$ is the absorption spectrum of the acceptor, $f(\lambda)$ is the normalized fluorescence emmission spectrum of the donor, and κ an orientation factor. Actual calculations show R_o = 37 Å but due to uncertainties in some of the approximations made, the range could be between 25-40 Å. Other estimates as to distance interactions between electron transfer proteins from theoretical calculations, computer calculated interactions between known structural proteins, and mere speculation from the structures of the individual proteins have been reported. These distances are summarized in Table I, where the references may be found.

The channeling of a reductant through a cleft to reach the oxidant in a direct collision or with bridging by a ligand (inner-sphere reaction) is not very likely since the metal is encased in a fixed, protective environment. This leaves the outer-sphere mechanism, which occur without the aid of a bridge (at distances slightly larger than defined by van der Waals contact radii,[11,12]) and the electron tunneling mechanism which seems a likely possibility for these systems.

Table I. Distances Postulated in Electron Transfer Protein Complexes.

Protein Complexes	Distance, Å	Speculator	Reference
cyt<u>c</u>-cyt<u>ox</u>	15-20	Erecinska	7
cyt<u>c</u>-cyt<u>ox</u>	25-40	Vanderkooi	6
cyt<u>c</u>-cyt<u>perox</u>	16.5	Kraut	8
cyt<u>c</u>-cyt$\underline{b}_5$	8.4	Salemme	1
cyt<u>c</u>-cyt<u>c</u>	4	Chien	4
cyt<u>c</u>-HIPIP	4-10	Bennett	9
cyt-chlor			
Chromatium	8	Hopfield	3
Chromatium	12-13	Jortner	10
Rhodapseudomonas	11	Hopfield	3

B. Theories of Electron Transfer

For electron transfer between species held at fixed distances, the rate can be delineated in terms of essentially independent electronic and nuclear parts. The actual distance between fixed centers becomes important in the contribution of the electronic part to the rate of electron transfer. The electronic part reaches its upper limit when the reactants are very close. In this case, the rate depends mainly on the nuclear part and the electron transfer is desinented as adiabatic. The lower limit of the electronic part radically decreases (typically by 5, 10, 15, or 20 orders of magnitude) when reactants are separated by large distances (10, 20, 30, or 40 Å, respectively).[13]

For the adiabatic nuclear contribution to the rate law, Marcus theory successfully describes the observed rates.[11,12,14,15] In this treatment the ligands remain intact and do not bridge the two metal atoms directly during the electron transfer. Such outer-sphere electron transfer reactions of moderate driving force have rates determined by: 1) the inner-sphere reorganization energy, which is dependent on the Franck-Condon barrier, 2) the outer-sphere reorganization energy, consisting mainly of the changes in electrostatic interactions of solutes and solvent in the formation of the activated complex, 3) the work terms for bringing reactants together and separation the products of the activated complex, and 4) the effect of the driving force for the electron transfer. Theory then predicts the following dependence for the rate constant:

$$k = \kappa \frac{kT}{h} \frac{Q^{\ddagger}}{\pi_i Q_i} e^{-E_a/RT} \qquad (2)$$

where κ is a thermally averaged transmission factor being equal to one for purely adiabatic behavior, Q's are the partition functions, and E_a is the activation energy. Expressing equation (2) in terms of free energy this expression becomes:

$$k = \kappa \frac{kT}{h} e^{-\Delta G^{\ddagger}/RT} \tag{3}$$

Marcus-type behavior now appears in terms of $\Delta G^{\ddagger}$:

$$\Delta G^{\ddagger} = \Delta G^{\ddagger}_{trans} + \Delta G^{\ddagger}_{in} + \Delta G^{\ddagger}_{out} + w_r + \Delta G_o/2 \tag{4}$$

Where $\Delta G^{\ddagger}_{trans}$ is the free energy of formation of the transition state:

$$\Delta G^{\ddagger}_{trans} = -RT\ln(hZ/kT) \tag{5}$$

where Z is the collision frequency.

The terms $\Delta G^{\ddagger}_{in}$ and $\Delta G^{\ddagger}_{out}$ are the reorganization energies of the inner- and outer-coordination shells, respectively:

$$\Delta G^{\ddagger}_{in} = \frac{3f_1 f_2 (a_1 - a_2)^2}{(f_1 + f_2)} \tag{6}$$

$$\Delta G^{\ddagger}_{out} = \frac{(\Delta q)^2}{4}\left(\frac{1}{2a_1} + \frac{1}{2a_2} - \frac{1}{d}\right)\left(\frac{1}{n^2} - \frac{1}{D_s}\right) \tag{7}$$

where q_1, q_2, a_1, and a_2, are the charges and radii of the two reactants respectively; d is the distance between the two reactant centers in the activated complex, with f_1 and f_2 the reactant force constants. The optical dielectric constant, n^2 and D_s, the static dielectric constant represent the contribution of the medium to the reorganization energy.

The w_r term in equation (4) is the work required to bring the reactants together, being calculated by Debye-Huckel treatment:

$$w_r = \frac{q_1 q_2}{D_s d(1 + \beta d\sqrt{\mu})} \tag{8a}$$

$$\beta = \left(\frac{8\pi n^2 e^2}{1000 D_s RT}\right)^{\frac{1}{2}} \tag{8b}$$

where N is Avogadro's number and μ is the ionic strength.

The thermodynamic drive likewise influences the activation free energy. By virtue of the parabolic shape of the two interacting potential functions, the change in $\Delta G^{\ddagger}$ is half that in ΔG_o.

When such a treatment is made with the electron transfer systems of $Fe(H_2O)_6^{2+/3+}$, $Ru(NH_3)_6^{2+/3+}$, $Ru(NH_3)_5(pz)^{2+/3+}$, $Ru(bpy)_3^{2+/3+}$, (where pz is pyrazine and bpy is bipyridine) good agreement is found between $\Delta G^{\ddagger}_{calc}$ and $\Delta G^{\ddagger}_{obs}$.[16] The distances between centers in these systems varies from 7 to 14 Å. In a system such as $Ru(bpy)_3^{2+/3+}$, the overlap between metal t_{2g} and ligand π^* orbitals is sufficient to allow adiabatic electron transfer at 14 Å between centers.

The electronic portion of the electron transfer rate would be expected to contribute significantly at greater distances than those allowed by outer-sphere electron transfer or where an insulating wall of protein prevents the metal coordination spheres of the prosthetic group from overlaping. The electronic portion is treated by Hopfield's theory of nonadiabatic, vibronically coupled electron transfer.

The theoretical model of Hopfield's rate equation is based on electron transfer between two sites in a fixed geometry. The electron to be transferred is initially in a wave function ψ_a, eventually to be transferred to site b in ψ_b. The matrix element, T_{ab}, represents the Hamiltonian of these two, one-particle states resulting from the overlap between these wave functions. The closer together sites a and b are, the greater the orbital overlap and the larger T_{ab} will be.

The rate of electron transfer on further development becomes dependent on the inter- and intramolecular vibrations, by giving an energy width to the electronic states. In a description analogous to

that of the Forster treatment of excitation transfer,[17,18] this rate can be expressed by:

$$k_{ab}^{u} = (2\pi/h)|T_{ab}(r)|^2 \int_{\infty}^{\infty} D_a(E) D_b'(E) dE \qquad (9)$$

with T_{ab} a function of the distance, r, of separation between sites a and b. The terms $D_a(E)$ and $D_b(E)$ are the electron removal and electron insertion spectral distribution functions, respectively. Assuming the curvature of the wave functions (k_a and k_b) are the same with or without the electron, $D_a(E)$ and $D_b(E)$ being also Gaussian shaped functions, the rate equation is restated as:

$$k_{ab}^{u} = (2\pi/h)|T_{ab}(r)|^2 (2\pi h^2)^{-\frac{1}{2}} e^{-(E_a - E_b - \Delta)^2/2\sigma^2} \qquad (10a)$$

where

$$\sigma^2 = (k_a q_a^2/2) k_B T_a \coth(T_a/2T) + (k_b q_b^2/2) k_B T_b \coth(T_b/2T) \qquad (10b)$$

and

$$\Delta = k_a q_a^2/2 + k_b q_b^2/2 \qquad (10c)$$

with q_a and q_b being the nuclear coordinates and k_B is the Boltzmann constant. The vibronic coupling parameter is defined by Δ, and T is the temperature in degrees Kelvin, with $k_B T_a$ ($k_B T_b$) being the energy separation between nuclear harmonic oscillator states for site a(b). At high temperature this rate becomes:

$$k_{ab}^{u} = (2\pi/h)|T_{ab}(r)|^2 (4\pi k_B T \Delta)^{-\frac{1}{2}} e^{-(E_a - E_b - \Delta)^2/4k_B T} \qquad (11)$$

In such a treatment, the electron transfer occurs from one vibronic state of a to another state of b, the vibrational form being that of a harmonic oscillator. The vibrational potential energy, $\frac{1}{2}kq^2$, relates k and q as the force constant and displacement from equilibrium nuclear position, respectively. The tunneling matrix element is further approximated by:

$$T_{ab} \simeq \frac{2.7}{(N_a N_b)^{\frac{1}{2}}} e^{-0.72r} \qquad (12)$$

which is the π resonance integral for carbon atoms, each in an aromatic molecule, with $(N_a N_b)^{-\frac{1}{2}}$ being a normalization factor of N_a and N_b atoms in contact through one "edge". The separation between edge atoms is then r. This π resonance integral is used as an approximation to comply with the cytochrome systems investigated.

Rates are reproduced in this treatment from 60 to 300 K for the electron transfer from a cytochrome to chlorophyll in Chromatium,[19,20] in which the parameters, $E_a - E_b = 0.05$ eV, $\Delta = 1.0$ eV, and $|T_{ab}| = 4 \times 10^{-4}$ eV, gives a transfer distance between heme groups of 8 Å. In a similar treatment with Rhodopseudomonas gelatinosa, also involving electron transfer via cytochromes, $E_a - E_b = 0.25$ eV,[21] with $T_a = T_b = 350$ K, $\Delta = 0.9$ eV and, $|T_{ab}| = 1 \times 10^{-4}$ eV which gives the transfer distance as 11 Å.

Previously, most correlations have been based solely on theoretical calculations. James Chien just recently completed an electron transfer study involving biological molecules in solution.[4] In this treatment, experimentally obtained kinetic data were found to be in good agreement with the theoretical rate constants predicted by Hopfield theory. By using metal substituted hemoproteins, the oxidoreductions of an iron heme and a metal-substituted heme was followed.

Treatment of such a system was extended to describe bimolecular electron transfers in solution. The rate of transfer is calculated by averaging the rate as a function of distance over probability distribution of geometries, where the relative location of donor and

acceptor varies with time. Neglecting a particular geometry for electron transfer, the bimolecular rate becomes:[22]

$$k_{ab}^{b} = 6.023 \times 10^{-4} k_{ab}^{u} (2\pi\lambda^3 r/R_p) \tag{13}$$

where λ is the characteristic decay constant defined by $\frac{1}{2}(1/0.72) = 0.7$ Å. The separation between interacting proteins is given by R_p. Activation parameters were shown to be:

$$\Delta H^{\ddagger} = (E_a - E_b - \Delta)^2/4 - 3RT/2 \tag{14}$$

$$\Delta S^{\ddagger} = R\ln\left[\frac{2.38 \times 10^{-2}}{k_B T}\left(\frac{2\pi\lambda^3 r}{R_p}\right) + \left(\frac{1}{4\, k_B T \Delta}\right)^{\frac{1}{2}} |T_{ab}|^2\right] - 3R/2 \tag{15}$$

The data used by Chien for comparisons between theory and observed values was taken from the literature when available. These values included midpoint potentials, vibronic coupling parameters, and distance of closest approach by x-ray structural data. When x-ray data was not available, space filling models were used to estimate the total distance. When rates were found to be independent of ionic strength then $k^{\mu} = k^{\infty}$; otherwise, equation (13) was corrected to allow for columbic interactions. This was corrected using Marcus theory in which k^{∞} is found from k^{μ} by the following relationship:

$$\ln k^{\infty} = \ln k^{\mu} + 3.58\left[\frac{e^{-\kappa R_a}}{1 + \kappa R_b} + \frac{e^{-\kappa R_b}}{1 + \kappa R_a}\right]\left(\frac{Z_a Z_b}{R_a + R_b}\right) \tag{16a}$$

$$\kappa = 0.329\mu^{\frac{1}{2}} \text{Å}^{-1} \tag{16b}$$

In this treatment, the values of $R_a(R_b)$, (the full radius of the molecule or the "active-site" radius) and $Z_a(Z_b)$ (between the total charges deduced from amino acid sequence or the "active-site" charge), are not so straightforwardly obtained. The "active-site" treatment was most consistent with rates extrapolated to infinite ionic strength. These results are summarized in Table II.

Table II. Rate Comparisons Between Theory and Experimental - From J.C.W. Chien Reference.

Electron Donor, a	Electron Acceptor, b	k^{∞}obs	k^{∞}calc	$\Delta H^{\ddagger}$ obs	$\Delta H^{\ddagger}$ calc	$-\Delta S^{\ddagger}$ obs	$-\Delta S^{\ddagger}$ calc
Fe_{cytc}	Fe_{cytc}^{+}	8.1×10^{3}	1.2×10^{4}	7.0	4.9	17	23
Fe_{cytc}	$Fe_{cyt_{551}}$	4.9×10^{4}	1.4×10^{4}	12	5.1	-12.4	23
$Fe_{cytc_{551}}$	Fe_{cytc}^{+}	4.9×10^{4}	2.1×10^{4}	12	5.1	-12.4	23
Co_{cytc}	Fe_{cytc}^{+}	8.3×10^{3}	9.6×10^{3}	2.3	3.7	33	23
Fe_{cytc}	$Fe(CN)_6^{3-}$	4.0×10^{6}	2.9×10^{6}	2	3.1	21	19
Fe_{cytc_2}	$Fe(CN)_6^{3-}$	5.6×10^{5}	4.9×10^{5}	11.4	3.7	-1.8	19
$Fe(CN)_6^{4-}$	$Fe_{cytc_2}^{+}$	2.2×10^{3}	1.7×10^{3}	5.2	6.2	10.2	19
$Fe(EDTA)^{2-}$	Fe_{cytc_2}	2.1×10^{4}	1.6×10^{4}	6.0	3.4	20	26
Co_{cytc}	$Fe(EDTA)^{-}$	46	45	4.2	5.0	36	31
Co_{cytc}	PM^{+}	5.2×10^{4}	1.1×10^{5}	6.3	5.4	18	18

[a]Independent of ionic strength, otherwise k obs was corrected to infinite ionic strength.

$k = M^{-1}s^{-1}$; $\Delta H^{\ddagger}$ = kcal/mole; $\Delta S^{\ddagger}$ = eu

From this data, the rates are in good agreement with those predicted by Hopfield's theory of vibronically coupled electron tunneling. It should also be mentioned that the activation parameters were in good agreement, with the exception of three cases. Chien suggests that the deviations result from some conformation change of one or both protein molecules.

Tunneling mechanisms have been postulated to describe electron transfer at distances of 40 Å. Likewise, experimental support now exists for tunneling at distances as short as 4 Å. It is the purpose of this study to help determine at what distances between redox centers that a particular mode of electron transfer dominates. Such an experiment requires a systematic separation of redox centers by progressively larger distances through a saturated ligand system in which distances are well defined and static throughout the electron transfer process. The rational to this system's design follows.

C. Characteristics of the Model System

The system so chosen for this investigation consists of a substitution inert ruthenium complex, and a substitution inert cobalt complex, each being fixed at chosen sites on a series of cholestane derivatives. Each complex-cholestane derivative may also be covalently bound to a treated silica gel. This system is diagrammed in Figure 3.

In such a ligand system, two metal atoms can be bound at well defined distances, as the cholestane system is rigid. The choice of a saturated system likewise precludes any likelihood of inner-sphere transfer of an electron. The number of existing cholestane derivatives also provides a wide choice of positions for metal binding, and consequentally a range of distances.

Figure 3. Diagram Depicting the Systems Chosen for this Investigation.

A = $-CH_3$
= $-CH_2CH_2-Si\equiv$

B = Other $-NH_2$ sites available for metal binding.

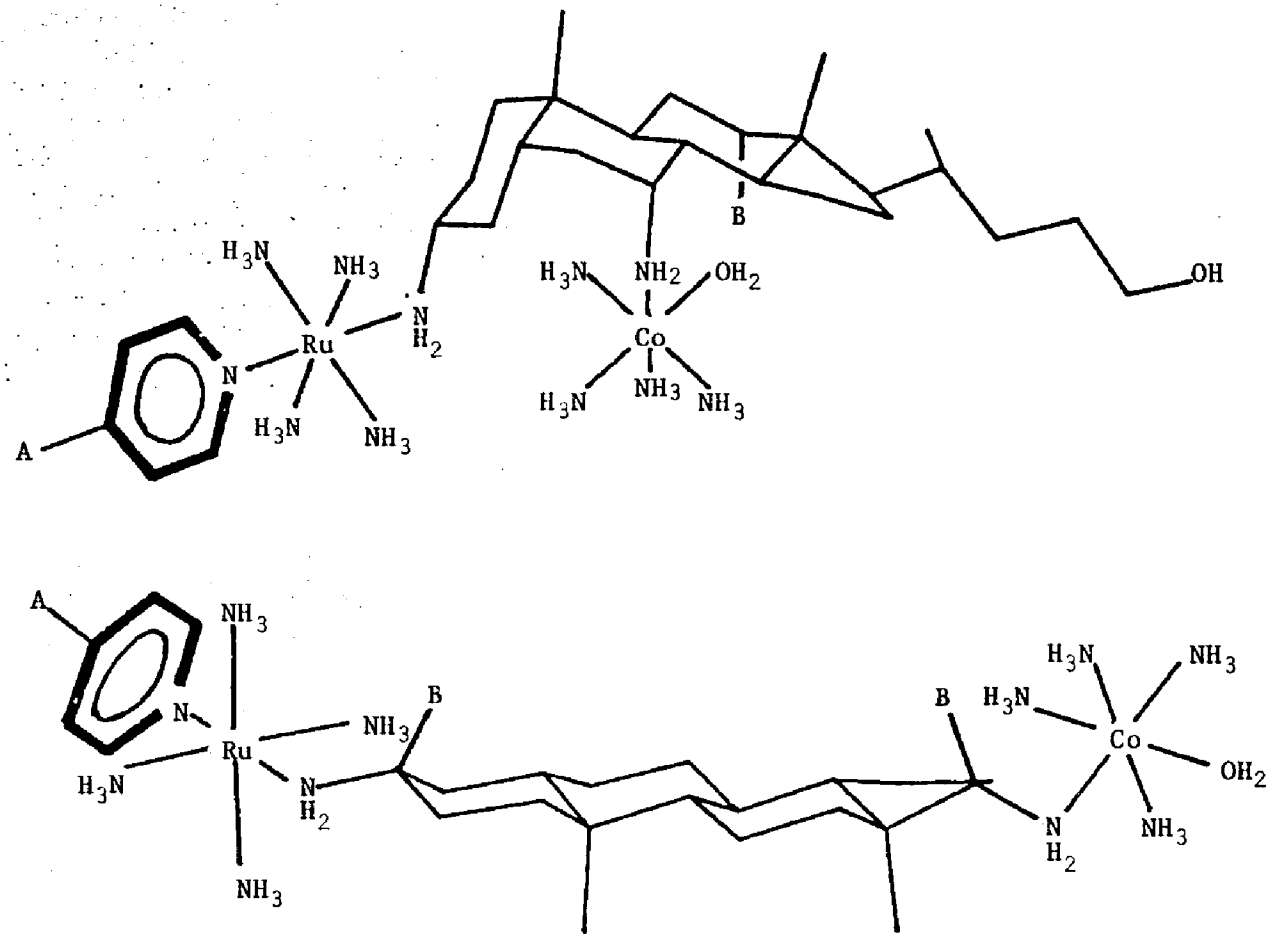
H3N
NH3
N
H2
Ru
N
H3N
NH3
A
B
H3N
NH2
OH2
Co
H3N
NH3
NH3
OH
A
NH3
N
Ru
H3N
NH3
B
N
H2
NH3
B
H3N
NH3
Co
H3N
OH2
N
H2
NH3

Figure 4. Diagram Depicting the Kinetic Scheme for this Investigation.

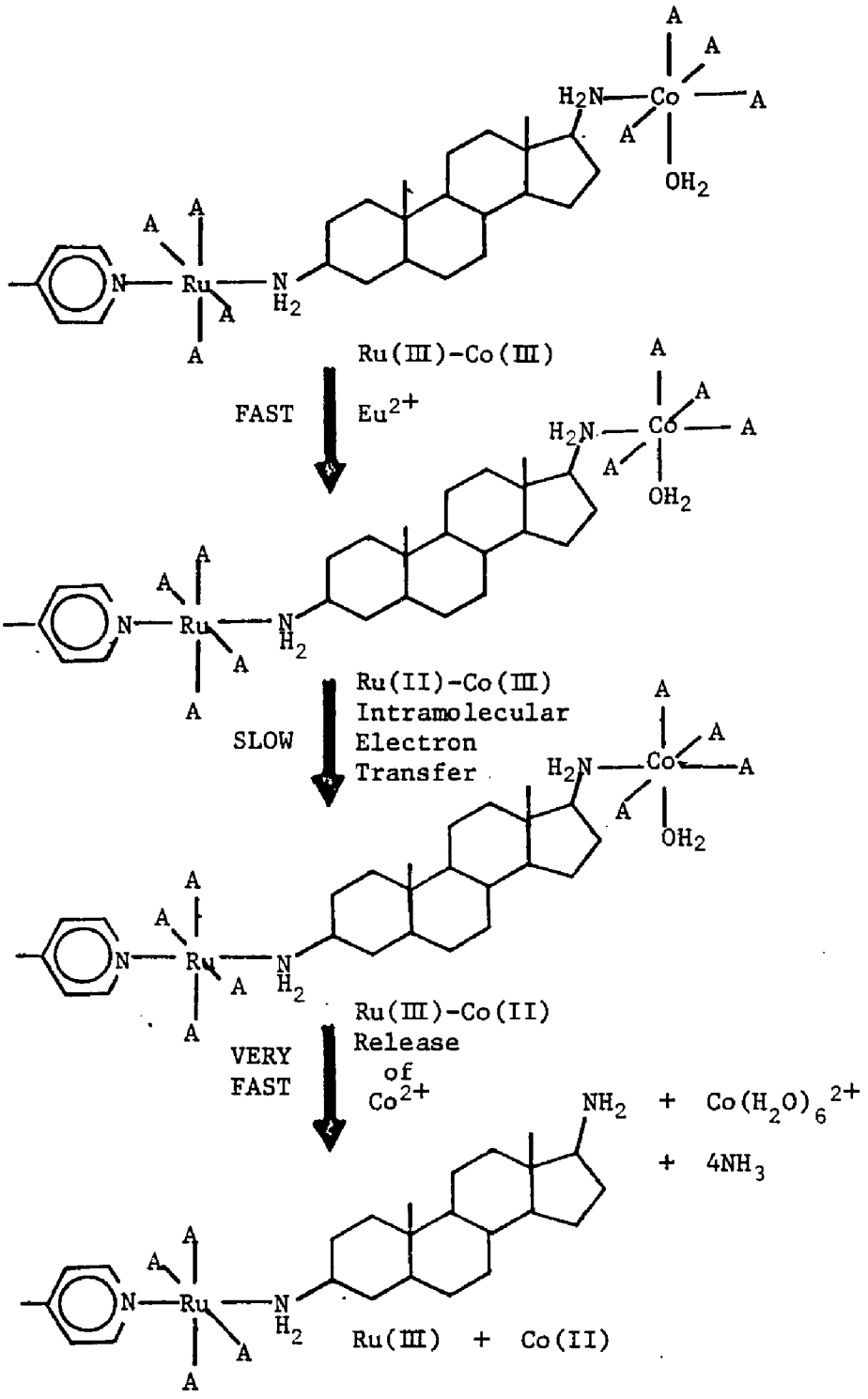
Ru(III)-Co(III)
FAST
Eu^{2+}
Ru(II)-Co(III)
Intramolecular
Electron
Transfer
SLOW
Ru(III)-Co(II)
Release
of
Co^{2+}
VERY
FAST
NH_2 + $Co(H_2O)_6^{2+}$
+ $4NH_3$
Ru(III) + Co(II)

The metals of choice are substitution inert. Both ruthenium (II) and (III) are substitution inert. The cobalt (III) site is also inert to substitution. Once the Co(III) complex has been reduced to Co(II) a labile species is produced. This lability may be utilized by monitoring the Co(II) species formed with the aid of a colorimetric reagent, or by conductivity measurements.

The initial state of the bimetallic complex involves Ru(III) and Co(III). Inherent in this system is the selective control of initiating rapid reduction of one of the metal atoms over the other. The Ru(III) is first reduced rapidly by a separate species (eg. Eu^{2+} or $Ru(NH_3)_6^{2+}$). Once this is done, the rate observed is the transfer of this reduced metal atoms's electron (Ru^{2+}) to the other metal atom (Co^{3+}). The choice of Co(III) in the starting complex is convenient since reduction is slow compared to that of Ru(III).[23,24,25] A high Franck-Condon barrier for inner-sphere rearrangement explains this observation.[26,27,28] The Ru(II) then reduces the Co(III) site intramolecularly. See Figure 4 for schematics.

Finally, attaching the complex to a gel provides two advantages. First, as the oxidant-reductant site separation increases, the rate of intramolecular electron transfer for nonadiabatic behavior should rapidly decrease. This increases the possibility of a bimolecular, intermolecular electron transfer to compete with the intramolecular transfer of interest. Fixing the complex to the gel will prevent such a complication.

One other complication is the possibility of the following reaction, which was observed in a similar system studied by Isied and Taube:[22]

$$Ru(II)LCo(III) + Ru(III)L \rightarrow Ru(II)L + Ru(III)LCo(III) \quad (17)$$

Such a condition is once again avoided by attaching the reactive species to a gel since the Ru(III)L product formed will be prevented from going into solution.

In this series of reactions, the nature of the first coordination sphere about the metal atom will remain constant; therefore, $\Delta G^{\ddagger}_{trans}$, $\Delta G^{\ddagger}_{in}$ and $\Delta G_o/2$ will not appear in this treatment as contributing factors in rate comparesons. The ratio of rates, if Marcus type behavior dominates, will be a function of distance (due to different outer-sphere reorganization energies described by equation (6)). In a Marcus treatment, the coulombic work term as shown in equations (8a) and (8b) also has a distance dependence which would normally contribute to the rate as seen in equation (4). For intramolecular reactions, of these complexes, there should be no coulombic work as distance is increased between reaction centers. Adiabatic electron transfer rates of these systems should increase with increasing separation due to electrostatic considerations. See Figure 5.

Activation parameters for tunneling reactions can be treated similarly to the method of Chien. The functional form of $|T_{ab}(r)|$ in this treatment is determined by an exponential decrease as oxidant-reductant separation increases. The slope of such a decrease would depend greatly on the exponential function of the tunneling matrix element. (See also Figure 5).

The discription of the synthesis of two steroid derivatives and a generalized synthetic scheme which may be applied to both free ion and silica bound forms of these bimetallic complexes follows. Initial

Figure 5. Theoretical Prediction of Rates as a Function of Distance

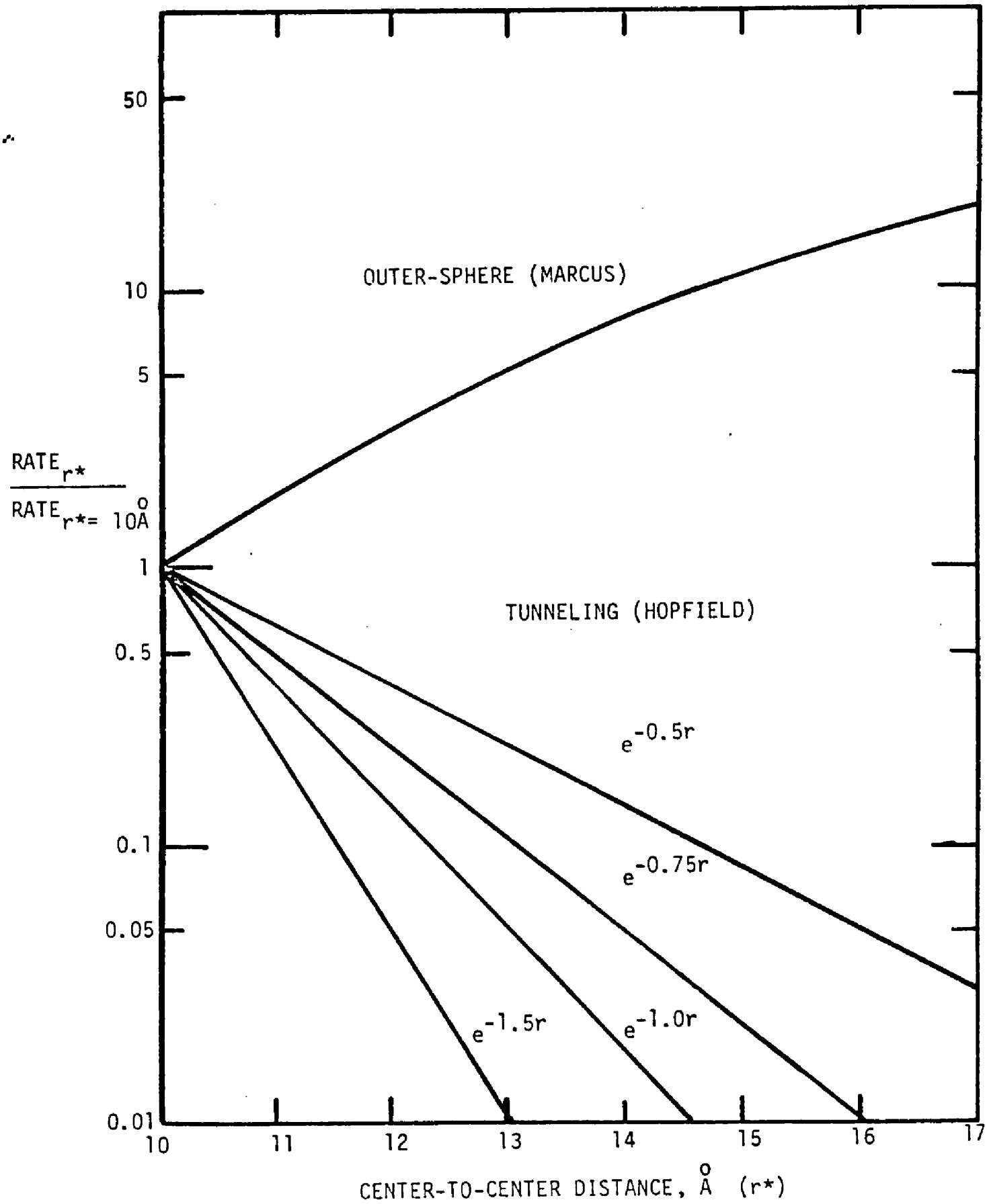
50
10
5
1
0.5
0.1
0.05
0.01
RATE r*
RATE r*= 10Å
OUTER-SPHERE (MARCUS)
TUNNELING (HOPFIELD)
e-0.5r
e-0.75r
e-1.0r
e-1.5r
10
11
12
13
14
15
16
17
CENTER-TO-CENTER DISTANCE, Å (r*)

kinetic studies were performed to test the schematic sequence diagrammed in Figure 4. This thesis should be viewed as a preliminary study since the complexity of such an investigation requires many approaches. This work represents the beginning of a series dedicated to the thorough study of electron transfer as a function of distance.

CHAPTER 2

EXPERIMENTAL

A. Materials

The materials used in this investigation are listed in Table III. All chemicals used were reagent grade, unless otherwise specified. Several of the solvents used were further treated from the reagent grade stock.

Trifluoromethansulfonic acid was fractionally distilled using a Vitro glassware set up.

Tetrahydrofuran was purified by refluxing a .5% suspension of CuCl in tetrahydrofuran for 30 minutes, followed by distilling. This was again refluxed with sodium metal, then with lithium aluminum hydride, followed by distillation over molecular sieves.[29]

Xylene was first purified in a separatory funnel by washing with concentrated H_2SO_4 until the yellow color was no longer detected in the acid layer. It was then dried over phosphorous pentoxide and distilled over molecular sieves.[29]

Acetone was fractionally distilled from potassium permanganate and stored over molecular sieves.

Some of the compounds used in the synthesis and kinetic investigations were also prepared from reagent grade and/or purified precursors.

$Ba(CF_3SO_3)_2$. Ten grams of $BaCO_3$ were suspended in 100 ml of water. Concentrated CF_3SO_3H was added drop by drop with vigorous stirring and warming until the solution cleared. Powdered $BaCO_3$ was added until no further fizzing was observed. This solution was filtered, and the solvent evaporated using a rotary evaporator.

Table III. Materials

Acetic Acid	Fisher
Acetone	Fisher
Acetonitrile	Fisher
Alumina(80-200 mesh)	Fisher
Ammonium Acetate	Fisher
Ammonium Carbonate	Fisher
Ammonium Hydroxide	Fisher
Androstanolone	Aldrich
Argon(prepurified grade)	Union Carbide
Ascorbic Acid	Aldrich
Barium Carbonate	Fisher
Chenodeoxycholic Acid	Aldrich
Chloroform	Fisher
Chromic Perchlorate	Frederick Smith Co.
Chromium Oxide	Alfa
Cobalt Carbonate	Alfa
Cobaltous Chloride	Fisher
Cuprous Chloride	Mallinckrodt
Cyclohexanone	Eastman
Dimethyl Sulfoxide	Fisher
Ethanol(95%)	Fisher
Ethanol(absolute-Gold Shield)	IMC Chemical Group
Ether(anhydrous)	Fisher
Europium Oxide	Alfa
Fluorochemical Acid	Fluorad

Hydrochloric Acid	Fisher
Hydrogen Peroxide(30%)	Fisher
Lithium Aluminum Hydride	Alfa
Lubriseal	Arthur H. Thomas Co.
Mercuric Chloride	Fisher
Mercury Metal(triple distilled)	Arthur H. Thomas Co.
4,4-diaminodicyclohexylmethane	Pfaltz & Bauer
Methanol	Fisher
4-morpholineethanesulfonic Acid	Aldrich
Nitrogen(prepurified grade)	Union Carbide
Trimethylorthoformate	Aldrich
Perchloric Acid	Fisher
Phosphorous Pentoxide	Fisher
Polyacrylamide Gel(Bio-Gel P-2, 100-200 mesh)	Bio-Rad
Potassium Permanganate	Merck
Potassium Thiocynate	Fisher
Resin(AG 2-X8, 50-100 mesh, chloride form)	Bio-Rad
Ruthenium Hexammine Trichloride	Matthey Bishop Inc.
Sieves(3 Å)	Davison
p-Toluenesulfonic Acid, Monohydrate	Baker
Trimethylchlorosilane	Petrarch Systems Inc.
Hexamethyldisilazane	Petrarch Systems Inc.
Silica Gel(60-200 mesh)	Davison
β-Trichlorosilyl-4-ethylpyridine	Petrarch Systems Inc.
Sodium Acetate	Fisher
Sodium Bisulfite	Fisher

Sodium Carbonate	Fisher
Sodium Carboxylate	Fisher
Sodium Cyanoborohydride	Fisher
Sodium Hydroxide	Fisher
Sodium Metal	Alfa
Sodium Sulfate	Fisher
Tetrahydrofuran	Fisher
Xylene	Fisher
Zinc Metal(granular, 20 mesh)	Fisher
Zinc Metal(mossy)	Baker

Sodium tosylate. Twenty grams of p-toluenesulfonic acid were treated with sodium hydroxide until the pH turned basic. Crystalline toluenesulfonic acid was again added until the pH just turned acidic. This solution was taken to dryness. The remaining product was dried overnight at 70°C in a vacuum oven.

Eu^{2+} solutions. One half hour prior to initiation of the kinetic runs, 7 mg of Eu_2O_3 were weighed, added to 5 ml of a 2.25×10^{-2} M HCl solution, then heated and stirred until dissolved. This solution was diluted to 10 ml, and poured onto a zinc amalgam and placed on the argon line equipped with a chromous bubbler.

Chromous bubbler. A 0.2 M chromic solution was prepared from chromic perchlorate and 0.5 M $HClO_4$. Meanwhile, 70 g of mossy zinc were added to a 4 M $HClO_4$ solution. After the mixture had bubbled vigorously for several minutes, the liquid was decanted, the zinc was rinsed with water, and dried on a paper towel. To 75 ml of a saturated $HgCl_2$ solution, 30 g of the cleaned zinc were added, and allowed to stand for a half hour. The amalgam was collected, dried, and placed into a gas dispersion bottle containing 250 ml of the chromic solution. This solution was bubbled with argon until a sky blue solution was observed, then the tower is ready for use.[30]

4,4-diaminodicyclohexylmethane. The brown waxy solid was dissolved in a minimum amount of methanol. Distilled water was then added drop-by-drop until no further precipitation of the white suspension was observed.

Figure 6. Inert Gasline Apparatus.

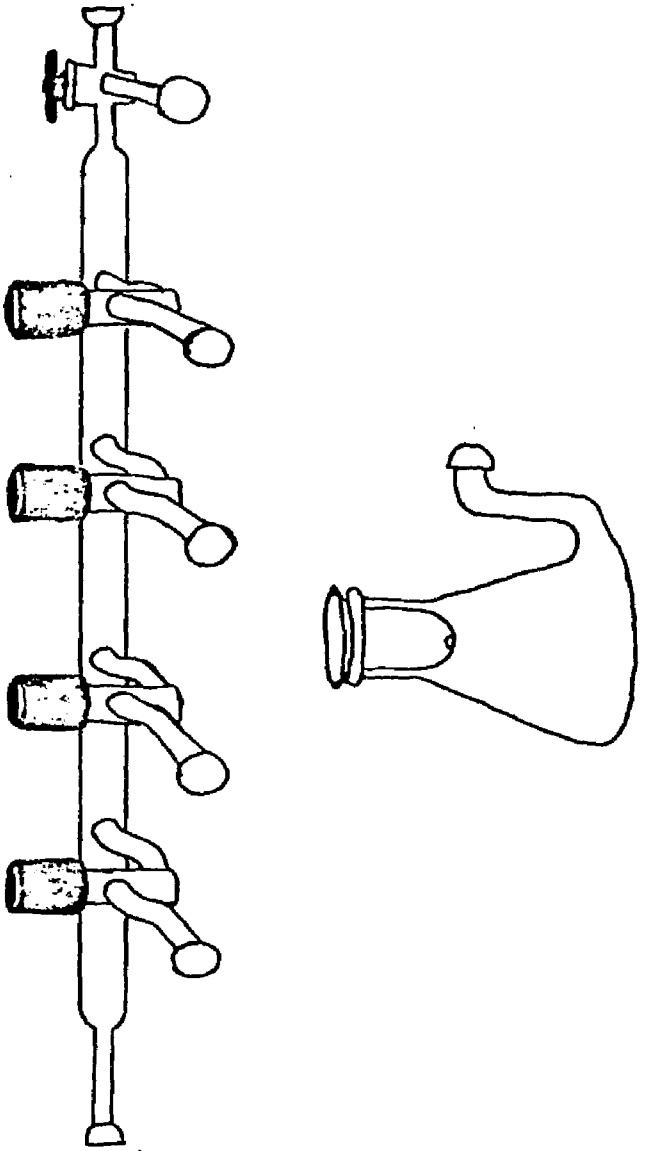

B. Synthesis

Organic Compounds

Methyl 3α,7α-dihydroxy-5β-cholanate

To 50 ml of freshly destilled methanol, 3 ml of concentrated HCl and 5 g of 3α,7α-dihydroxy-5β-cholanic acid (chenodeoxycholic acid) were added. This solution was refluxed for one half hour, and cooled to room temperature. After cooling, 10 ml of water were added, and the solution was evaporated until a precipitate was observed. Another 40 ml of water were added. Two pellets of NaOH were added, and the solution was extracted with chloroform. The chloroform layer was saved and the ester was collected by evaporating this layer.

Methyl 3,7-diketo-5β-cholanate

A solution of 4 g of CrO_3 in 15 ml of water was first prepared. Six grams of the methyl dihydroxycholanate were dissolved in 15 ml of glacial acetic acid. A few milliliters of glacial acetic acid were added to the CrO_3 solution followed by the drop-by-drop addition of the cholanate solution. A deep brown solution soon resulted. The solution was stirred for 15 minutes after the last addition of cholanate solution had been made. Water was added to precipitate the product. The product was dissolved in methanol and reprecipitated with water.

Methyl 3α,7α-diamino-5β-cholanate

Six grams of the diketocholanate were added to 50 ml of methanol followed by 16.2 g of ammonium acetate, and 4 g of $NaBH_3CN$. This was stirred for 48 hours. The product was extracted into chloroform and was collected by evaporating the dried chloroform layer.

3α,7α-diamino-5β-cholan-24-ol

Dried tetrahydrofuran was used to dissolve 4 g of the diamino-cholanate. Two grams of lithium aluminium hydride were added to another 30 ml portion of THF. The cholanate solution was slowly added to the LAH solution, and the mixture was left to stand for two hours. Water was added a few drops at a time to the reaction solution until the solution clears and the precipitate settled to the bottom of the flask. The flask was kept in an ice bath during this procedure. After filtering, the solution was dried with Na_2SO_4 and then taken to dryness.

3,17-diketo-5α-androstane

This compound was prepared from androstanolone by the same methods described for the methyl 3,7-diketo-5β-cholanate synthesis.

3,17-dioxime-5α-androstane

An aqueous solution of 150 mg of hydroxyl amine hydrogen chloride and 200 mg of sodium acetate was prepared, to which 100 mg of the diketoandrostane were added. Enough ethanol was added to make a clear solution. This solution was refluxed for 5-6 hours. Excess ethanol was distilled off and the white crystalline product was filtered and dried.

3β,17β-diamino-5α-androstane

To a refluxing solution of the dioxime (100 mg) in isoprpoanol, 300 mg of sodium metal were added in portions. Water was added to this solution which was then extracted with chloroform. Evaporation of the $CHCl_3$ layer yielded a white solid which was recrystallized from methanol/ether or methanol/water.

[4,4-diaammoniumdicyclohexylmethane]Cl_2

Ten grams of the diaminodicyclohexylmethane were suspended in 100 ml of water. Concentrated HCl was added drop-by-drop with vigorous stirring and warming until the solution cleared. This solution was taken to dryness, and the resulting cake was washed with ether. Tables IVA. and IVB. follow with infrared spectra assignments for various organic products and synthetic intermediates.

Table IVA. Some Organic Infrared Assignments.

Assignment	3,7dkc	3,17dka	3,17kha
CH Stretch	2969 s 2947 s 2870 s	3006 s 2928 s 2852 s	3015 s 2932 s 2852 m
C=O Stretch	1735 s 1710 s	1720 s 1700 s	1700 s
CH Bend	1450 m 1431 m 1414 m	1508 m 1466 m 1442 m 1413 m	1512 m 1470 m 1445 m 1418 m

Table IVB. Diamine Infrared Spectra Assignments.

Assignment	$pacmCl_2$	3,7dac	3,17daa
NH Stretch	3440 m(b)	3160 s(b)	3300 m(b)
CH Stretch	2920 s 2623 w 2542 w	2980 s 2860 s 2320 m 2168 m	2920 s 2846 s
NH Bend	1601 m	1650 m(s) 1588 m	1590 m(b)
CH Bend	1488 m 1444 m 1352 m	1464 m 1443 m 1373 m	1444 m 1377 m

Intensities: w = weak, m = medium, s = strong

Descriptions: (b) = broad, (s) = shoulder

$pacmCl_2$ = [4,4-diamoniumdicyclohexylmethane]Cl_2
3,7dac = 3α,7α-diamino-5β-cholan-24-ol
3,7dkc = Methyl 3,7-diketo-5β-cholanate
3,17daa = 3β,17β-diamino-5α-androstane
3,17dka = 3,17-diketo-5α-androstane
3,17kha = Androstanolone

Cobalt Compounds

$[Co(NH_3)_5(dmso)][CF_3SO_3]_3$

In a method similar to that described by O'Halloran and Malin,[31] the trifluoromethanesulfonate analog to their perchlorate preparation was prepared. Infrared and NMR spectra matched those spectra seen by O'Halloran and Malin for this complex.

$[Co(NH_3)_4(CF_3SO_3)_2][CF_3SO_3]$

Initially, $[Co(NH_3)_4(H_2O)Cl]SO_4$ was prepared from $CoCl_2 \cdot 6H_2O$ by previously described methods.[32] Elemental analysis was confirmatatory for this product. Five grams of the chloroaquotetraammine cobalt complex were then dissolved in 30 ml of anhydrous CF_3SO_3H and a steady stream of N_2 was passed through the solution as it was warmed to 90°C. After evolution of HCl (monitored with a dilute solution of $AgNO_3$ in acetone) the flask was cooled in an ice bath. At this time the gas flow was discontinued and 50 ml of ether was added drop by drop with vigorous stirring. Further dilution resulted in a violet suspension, which was transferred to a capped centrifuge tube and centrifuged. The pellets were resuspended in ether and again centrifuged three times. They were then resuspended and filtered under vacuum in a sintered glass funnel. After further ether washes, the product was ground in a mortar and dried in vacuo over P_2O_5. This was similar to procedures described by Sargenson utilizing $CF_3SO_3^-$ as a labile ligand for Co(III) complexes.[33]

$[Co(NH_3)_4(H_2O)(L)][CF_3SO_3]_4$

A 75.8 mg sample of dry $[Co(NH_3)_4(CF_3SO_3)_2][CF_3SO_3]$ was dissolved in 10 ml of dry acetone. One equivalent of ligand (three equivalents in the case of 4,4-diaminodicyclohexylmethane), was added to the purple

acetone solution. A color change was observed from purple to rose, at which point the solution was taken to dryness and dissolved in an aqueous HCl solution at pH 4. This solution was then passed through a P-2 column. The orangish fraction was then taken to dryness. The ligand is verified by the sharp CH stretch at 2930 and 2850 cm^{-1}.

Figure 7. Spectrum of $[Ru(NH_3)_4(SO_4)(pic)]Cl$.

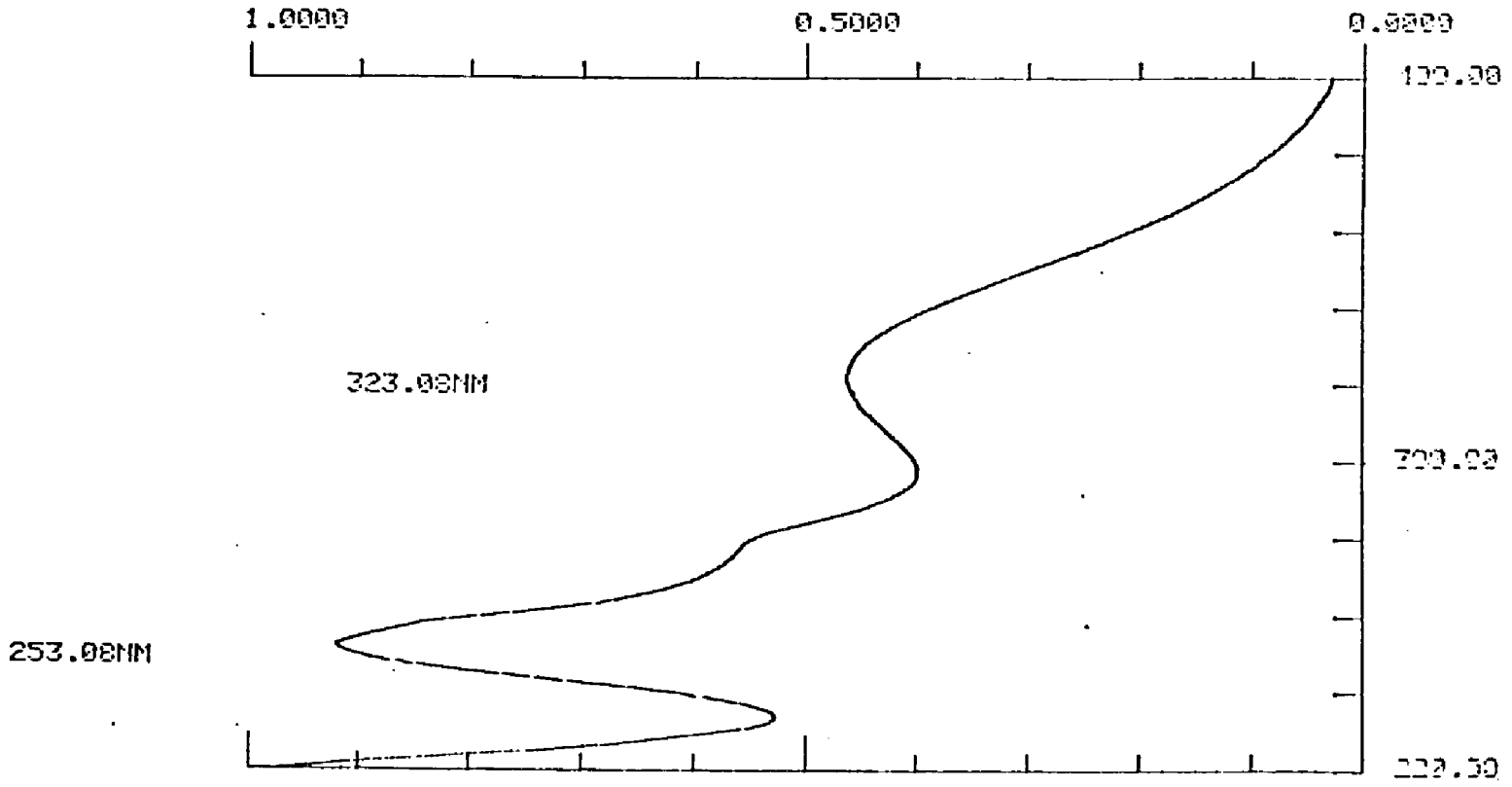
1.0000
0.5000
0.0000
323.00NM
253.00NM

Ruthenium Compounds

trans-$[Ru(NH_3)_4(SO_2)Cl]Cl$

The method of Wiberley[34] was used. Sulfur dioxide was generated by the drop by drop addition of 8 M H_2SO_4 to a slurry of 100 g of sodium sulfite. This sulfur dioxide was then bubbled at a controlled rate into the reaction flask.

$[Ru(NH_3)_4(SO_4)(pic)]Cl$

This species was prepared by the general procedure described by Isied.[26] A 90 mg sample of trans-$[Ru(NH_3)_4(SO_2)Cl]Cl$ was dissolved in 5 ml of water under argon, where a slight excess of γ-picoline was added drop by drop (3 drops). The addition of 80 mg of $NaHCO_3$ followed and the reaction was left to stand for three minutes (until bubbling subsided). Then four drops of 6 M HCl were added, followed quickly by addition of four drops of 30% H_2O_2. The solution was then quickly poured into acetone and placed in a freezer for several minutes. The product was filtered and washed with acetone and ether. The product spectrum is shown in Figure 7. This spectrum is very similar to the spectrum of trans-$[Ru(NH_3)_4(py)SO_4]Cl$ reported by Ford, et al..[35]

$[Ru(NH_3)_4(pic)(L)]Cl_4$

This is a general synthesis devised to work for all ligands used in the course of this study. In a 24/40 jointed erlenmeyer flask, 57 mg of $Ba(CF_3SO_3)_2$ and a slight excess of ligand (except for the case using 4,4-diaminodicyclohexylmethane where a three fold excess was used) was added. These two compounds were then dissolved in methanol, after which a large excess of Na_2SO_4 was added to the flask. Then 50.4 mg of $[Ru(NH_3)_4(pic)(SO_4)]Cl$ were dissolved in the methanol

solution. A bright yellow coloration occurs immediately. This solution was stirred for 15 minutes. The solution was then concentrated over Na_2SO_4 forming a cake. The product was recovered by redissolution in absolute ethanol followed by evaporating to dryness using a rotary evaporator. This orangish-yellow compound was then dissolved in a pH 4 aqueous solution of HCl, and was passed through a P-2 column. The product may be collected at this stage by exchanging anions to Cl^- with a Bio-Rad anion exchange column, and then pouring the resulting orangish solution into acetone.

Another alternative to the above method gives a larger yield. In a method similar to one used by Taube,[36] 60 mg of $[Ru(NH_3)_4(SO_4)(pic)]Cl$ in 30 ml of methanol were reduced with zinc amalgam under an argon atmosphere. This solution was transferred to an oxygen purged flask containing a slight excess of ligand (a five fold excess is used with 4,4-diaminodicyclohexylmethane). The reaction proceeded for 2 hours, after which the solution was made slightly acidic with 6 M HCl, and then treated with bromine water drop by drop until the color change from deep orange to pale yellow was observed. This solution was extracted with chloroform, concentrated to 5 ml, and precipitated in acetone. The product with 4,4-dicyclohexylmethane was further treated with several ethanol washes. A representative spectrum is shown in Figure 8. Table V. compares the similarities between uv-vis spectra of this complex series.

Figure 8. Spectra of $[Ru(NH_3)_4(pic)(3,7dac)]$ in oxidized (left most peaks) and reduced (right most peak) states.

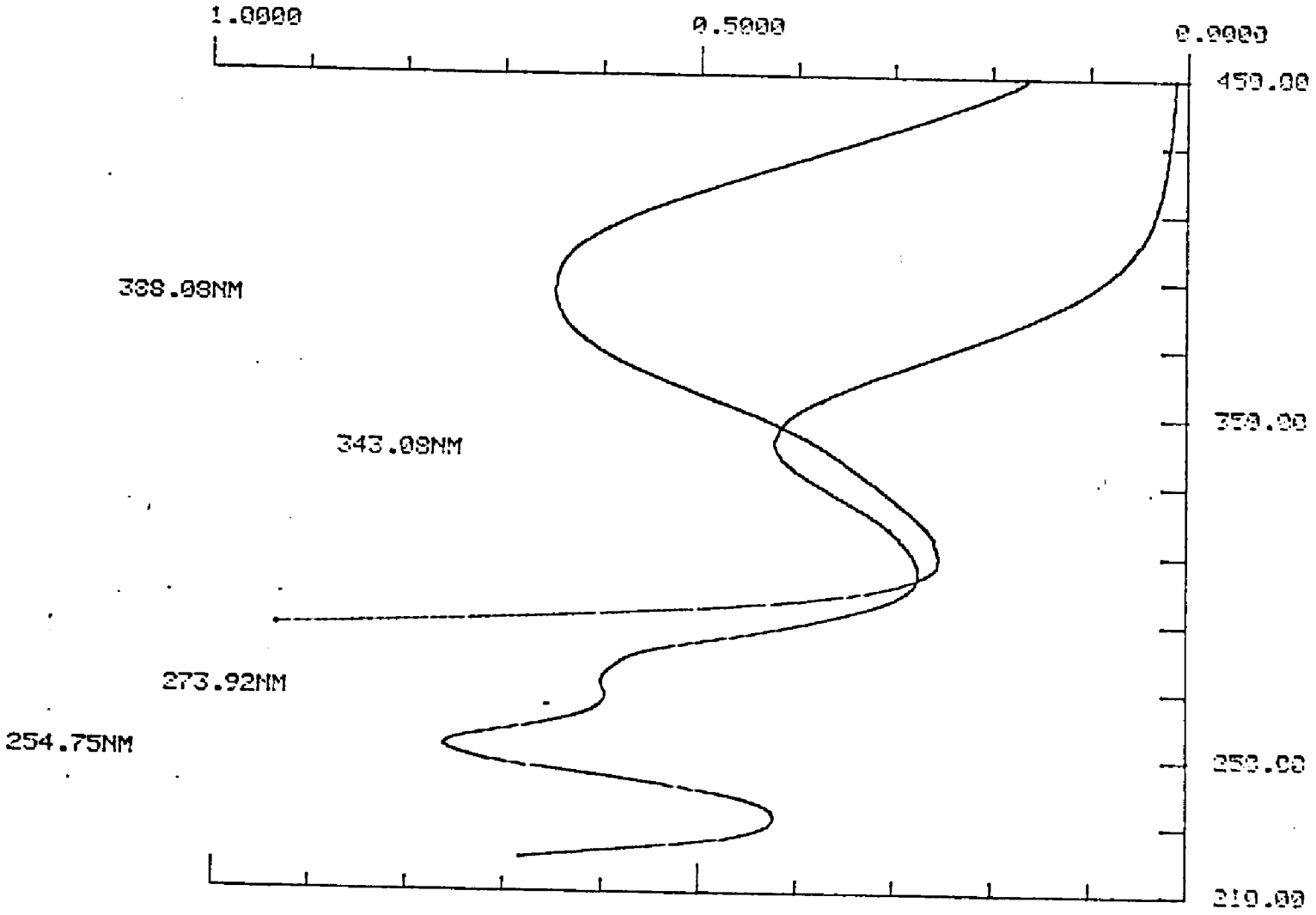
1.0000
0.5000
0.0000
450.00
350.00
250.00
210.00
338.08NM
343.08NM
273.92NM
254.75NM

Table V. UV-Vis Spectral Assignments

Compound	Abs(nm)	$\varepsilon \times 10^{-3}$ (lit/mole·cm)
$Ru(NH_3)_4(pic)(SO_4)$	253[a]	5.0
	323[b]	2.5
$Ru(NH_3)_4(pic)(3,7dac)(ox)$	253[a]	5.0
	344[b]	1.9
(red)	388[c]	4.3
$Ru(NH_3)_4(pic)(3,17daa)(ox)$	254[a]	5.0
	342[b]	2.3
(red)	389[c]	4.1
$Ru(NH_3)_4(pic)(pacm)(ox)$	254[a]	5.0
	345[b]	2.6
(red)	387[c]	3.8

Assignments for spectral types: a) $\pi \rightarrow \pi^*$(pic); b) L→Mπ(LMCT); c) M→Lπ(MLCT).

These assignments of ε are made by ratios of the $\pi \rightarrow \pi^*$ band to the assigned peaks. This value agrees to those reported in the literature.[35]

Binuclear Compounds

$[(pic)(NH_3)_4Ru(pacm)Co(NH_3)_4(H_2O)][CF_3SO_3]_6$

The $[Ru(NH_3)_4(pic)(pacm)]Cl_4$ was converted to the trifluoromethanesulfonate salt by using a Bio-Rad anion exchange column. Freshly distilled n-propanol was used to dissolve 68 mg of $[Ru(NH_3)_4(pic)(pacm)]-[CF_3SO_3]_4$. The bright yellow cloudy solution cleared upon addition of 132 mg (a three fold excess) of $[Co(NH_3)_4(dmso)][CF_3SO_3]_3$ to become lavender. After twelve hours, the solution was diluted with water to twice the original volume, and then concentrated using a rotary evaporator to 10 ml. This procedure was repeated until the odor of the propanol was no longer detected. The sample was then passed through a P-2 column, collected, and then washed with ether.

$[(pic)(NH_3)_4Ru(L)Co(NH_3)_4(H_2O)]Cl_6$

Utilization of labile $[Co(NH_3)_4(CF_3SO_3)_2][CF_3SO_3]$ was a more convenient method for forming the bimetallic complex. The previous $[Ru(NH_3)_4(pic)(L)]Cl_4$ product may be reconverted to the $CF_3SO_3^-$ salt by again using a Bio-Rad anion exchange column charged with CF_3SO_3H, and once again taking this product to dryness. At this point, dry product was redissolved in 10 ml of very dry acetone to which a one-and-a-half fold excess of $[Co(NH_3)_4(CF_3SO_3)_2][CF_3SO_3]$ was added. This solution was stoppered and stirred for 45 minutes, taken to dryness, redissolved in a pH 4 aqueous HCl solution, and passed through a P-2 column. The product fraction was then passed through a Cl^- anion exchange column and precipitated in acetone. By following this alternate scheme, reaction times were reduced giving better yields. Product spectra obtained by either method are identical. See Figure 9.

Figure 9. Spectra of $[(pic)(NH_3)_4Ru(3,7dac)Co(NH_3)_4(H_2O)]Cl_6$. The right most spectrum is of the region characteristic of Co(III). The left portion of the figure shows the spectral region characteristic of Ru(III) and Ru(II). The left most peaks are in the oxidized state, the right most in the reduced state.

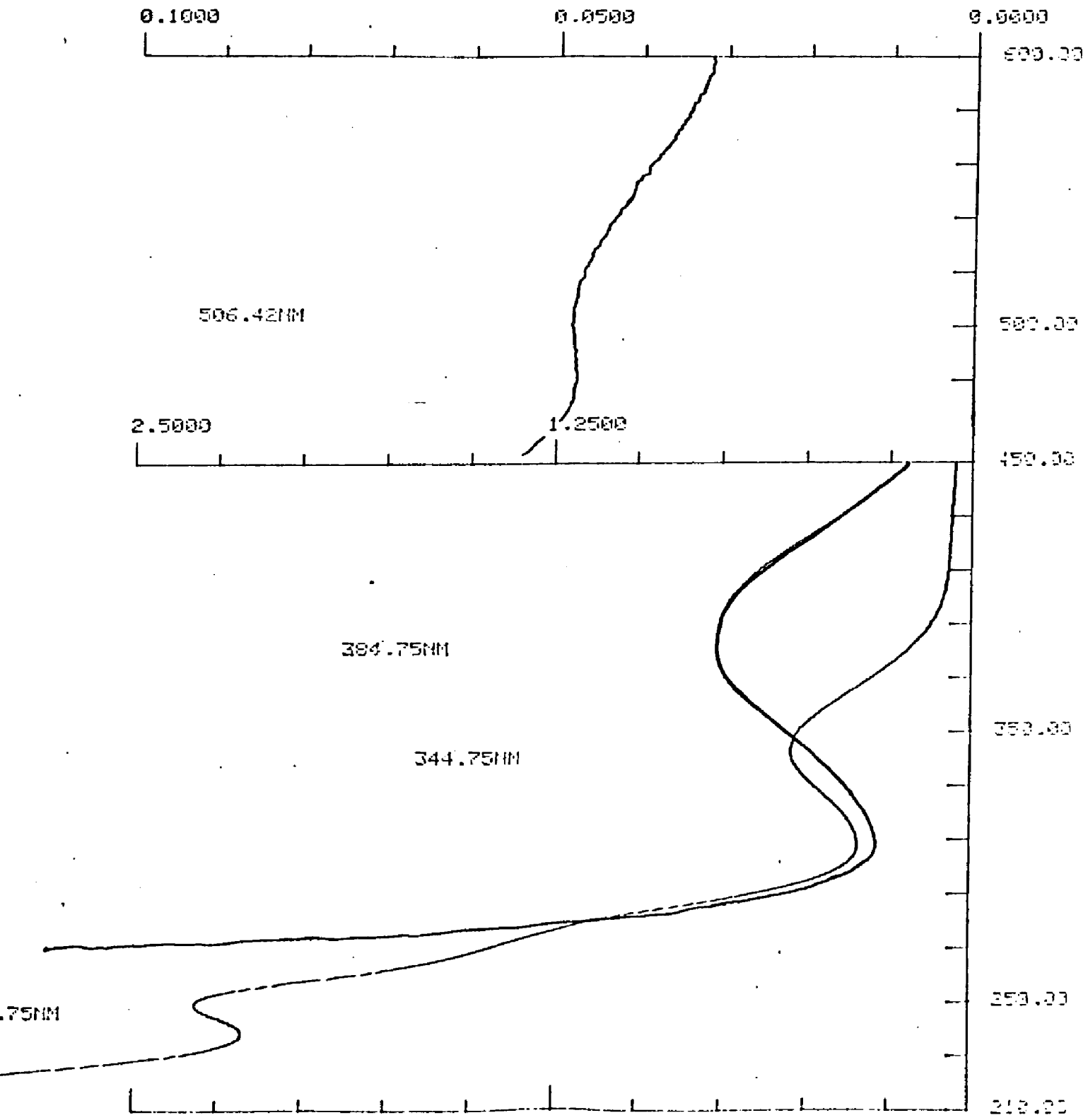
0.1000
0.0500
0.0000
500.00
506.42NM
500.00
2.5000
1.2500
450.00
384.75NM
350.00
344.75NM
.75NM
350.00
210.00

$\underline{[(H_2O)(NH_3)_4Co(L)Ru(NH_3)_4(pic)]Cl_6}$

The cobalt portion may be added before the ruthenium portion of the bimetallic complex by first dissolving about 75 mg of the $[Co(NH_3)_4(H_2O)(L)][CF_3SO_3]_4$ complex in 25 ml of methanol. An equivalent amount of $Ba(CF_3SO_3)_2$ and $[Ru(NH_3)_4(SO_4)(pic)]Cl$ was added to this methanol solution. Within two hours a clear yellow solution resulted. This solution was taken to dryness in the presence of Na_2SO_4 with the rotary evaporator, and then redissolved in absolute ethanol. The Na_2SO_4 was filtered from the ethanol solution, and this solution was once again taken to dryness. In a pH 4 aqueous HCl solution, the product was redissolved and passed through the P-2 column. This was once more passed through an anion exchange column charged with Cl^-. The product was most easily collected by then taking to dryness. Infrared data for the bimetallic complexes are listed in Table VI. Table VIII shows a cobalt:ruthenium ratio analysis.

The elemental analysis for the two bimetallic complexes are given as follows (Galbraith, Knoxville, Tenn.):

$[(NH_3)_4(H_2O)Co(3,7dac)Ru(NH_3)_4(pic)]^{5+}$

calculated:	C, 36.22	H, 7.60	Ru, 10.16	Co, 5.92
found:	C, 9.26	H, 4.80	Ru, 15.28	Co, 9.26

$[(NH_3)_4(H_2O)Co(3,17daa)Ru(NH_3)_4(pic)]^{5+}$

calculated:	C, 32.97	H, 7.41	Ru, 11.10
found:	C, 8.44	H, 4.37	Ru, 15.18

Table VI. Infrared Spectral Assignments for Bimetallic Complexes.

Assignments	Ru-pacm-Co	Ru-3,7dac-Co	Ru-3,17daa-Co
NH Stretch	3440 s(b) 3190 s(b)	3440 s(b) 3176 s(b)	3440 s(b) 3200 s(b)
CH Stretch	2922 s 2856 m	3018 s(s) 2811 s(s)	2930 m(s)
NH Bend	1618 m(b)	1622 m	1618 m
CH Bend	1518 w 1448 m 1400 m	1404 s	1400 s
-⟨⟩N Ring Stretch	1312 w 1301 w	1312 m 1302 m	1310 m 1300 m

Intensities: w = weak, m = medium, s = strong

Description: (b) = broad, (s) = shoulder

pacm = 4,4-diaminodicyclohexylmethane
3,7dac = 3α,7α-diamino-5β-cholan-24-ol
3,17daa = 3β,17β-diamino-5α-androstane

Table VII. Co:Ru Ratio Analysis for

$[(pic)(NH_3)_4Ru(L)Co(NH_3)_4(H_2O)]Cl_6$

Ligand	Ru analysis[a] (M)	Co analysis[b] (M)	Co:Ru
3,7dac	3.3×10^{-4}	3.06×10^{-4}	.93
3,17daa	3.3×10^{-4}	3.10×10^{-4}	.94
pacm	1.8×10^{-4}	2.13×10^{-4}	1.18

Calculations were based on: a) extinction coeffcients listed in Table V and b) extinction coeffcient of $Co(SCN)_4^{2-}$ in acetonitrile. The analysis was performed on the kinetics stock solutions by reduction with excess ascorbate overnight, taking to dryness and redilution to 3.00 ml with a solution of KSCN (0.01 M) in acetonitrile. The peak at 623 nm for Co^{2+} was compared to the pre-reduced stock solution peak at 345 nm.

Silica Gel Preparations

$\equiv Si(OCH_3)(CH_2CH_2-\text{Py})$

First, 23.0 ml of trichlorosilylethylpyridine and 4.8 ml of trimethoxymethane were refluxed in 100 ml of freshly distilled xylene for three hours. While the refluxing was continued, 10 g of very dry SiO_2 were added. After this addition, the refluxing was continued for 24 hours. The treated gel was filtered and washed with methanol and acetone and dried under a vacuum.

Gel Silylation

From coverage data observed by Burwell, et al.,[37] calculations show for every 10 g of the pyridyl gel, 50 ml of hexamethyldisilazane, and 5 ml of trimethylchlorosilane should be added. This reaction was stirred for eight hours. The silylized gel was then collected by filtration and washed with methanol and acetone.

Gel-Bimetallic Compounds

gel-⊛N-$Ru(NH_3)_4(L)Co(NH_3)_4(H_2O)$|

The gel compounds were also obtained by similar methods described in the preceding cobalt and ruthenium syntheses. For each 500 mg of pyridyl gel, 100 mg of $[Ru(NH_3)_4(SO_2)Cl]Cl$ were used in the initial step of the syntheses. All other reactants were used in the appropriate relative amounts. The only major change in technique was the use of propanol as the solvent for the ruthenium-ligand binding stage of the synthetic procedure. Throughout the entire synthetic procedure, an argon atmosphere was constantly maintained. The product gel was finally washed with acetone and dried under argon. Note: The ligand attachment stage must be accomplished through the $Ba(CF_3SO_3)_2$ route.

C. Methods and Techniques

Characterization of Gels

Treating a known weight of gel with an excess of ascorbate in 10 ml of water for 24 hours allowed the complete reduction of the metal sites. Pipetted 0.200 ml portions of the reduced gel solution were treated with 3.00 ml of a 0.01 M solution of KSCN in acetonitrile. The concentration of Co^{2+} was measured from the absorption at 623 nm from the visible spectrum.

The ruthenium(III) concentration was obtained from visible spectra. A 0.1 cm sample cell was prepared by suspending a known weight of the exhaustively reduced gel with an excess of SiO_2 in cyclohexanone after air oxidation. The volume of the suspension was then measured. Spectra were recorded over various sample areas by moving the cell by small increments. Molar absorptivities of the free ion species were used to calculate the concentration on the gel. See Table VIII.

Molecular Structures

Molecular calculations reported within were taken from the Prophet Molecules System.[38] This system is available through the National Institutes of Health, utilizing equipment supplied by Tektronix. Crystallographic data were entered from several sources. The data for the cis fused ring 3,7-cholestane coordinates were supplied from the x-ray structure reported for 3α,7α,12α-trihydroxy-5β-cholestan-26-oic acid.[39] The crystal structure used for the trans fused ring complex of the 3,17-androstane was obtained from the Public Molecules Table of Crystallographic Coordinates.[40] The cobalt complex coordinates were entered from the $Co(NH_3)_6^{3+}$ structure reported by Ibers.[41] Coordinates for the ruthenium complex were entered from data reported by Carol

Table VIII. Exhaustive Reduction Analysis on

gel-◎N-$Ru(NH_3)_4(pacm)Co(NH_3)_4(H_2O)^{6+}$

Species Analyzed	Solvent	λ nm	ε $\frac{\text{liter}}{\text{mole}\cdot\text{cm}}$	ΔOD	b cm	Concentration on gel
$Co(SCN)_4^{2-}$	aceto-nitrile	623	1580	0.153	1.00	1.33×10^{-4} mole/g[b]
gel-N-$Ru(NH_3)_4(pacm)^{4+}$	SiO_2 cyclo-hexanone slurry	365	2600[a]	1.594	0.10	1.51×10^{-4} mole/g[c]

[a]This ε is from absorption data for $(pic)Ru(NH_3)_4(pacm)^{4+}$ in water.

[b]The sample used in the cobalt analysis is 0.11661 g of gel in 10 ml reaction molume. A 0.200 ml volume is then treated with 3.00 ml of KSCN reagent.

[c]The sample used in the ruthenium analysis is 0.01363 g with a cell volume of 0.3356 ml.

Creutz the $Ru(NH_3)_5(pz)^{2+}$ structure.[42] All crystallographic data were tabulated and changed to cartesian coordinates through the public preconnect-QT command. The final molecular coordinates were obtained through the editmodel procedure.

UV-Visible, IR, and NMR Spectra

Kinetic runs were recorded on both the Cary 14 and Beckman DU-8 spectrophotometers. The UV-Vis spectra for the complexes reported within were recorded on the Beckman DU-8 spectrophotometer.

Infrared spectra were recorded on a Beckman 4240 recording spectrophotometer (range: 4000-250 cm^{-1}). The KBr disc method was used for all spectra.[43]

Proton NMR spectra were recorded on the Varian EM360A. The solvent chosen for these spectra was $CDCl_3$ with 1% tetramethylsilane. All spectra reported were recorded at room temperature.

Cyclic Voltammetry

The apparatus used for recording cyclic voltammograms consisted of a Bioanalytical CV-1A Cyclic Voltammetry Unit. An H-cell set up was used, with a coiled platinum wire for a working electrode, a second platinum wire as an auxiliary electrode, and a silver chloride electrode used as the reference. Voltammograms were recorded on an Onmigraphic 2000 X-Y recorder.

The half wave potentials, $E_{\frac{1}{2}}$, were calculated from the arithmetic average of the peak potentials. Measured potentials were converted to the NHE scale by adding +0.222 V to the measured $E_{\frac{1}{2}}$ values.

The cyclic voltammetry experiments were performed directly with the kinetic stock solutions being 0.1 M in ionic strength. These voltammograms were then compared with the voltammogram of $Ru(NH_3)_5(py)$.

This complex is known to be reversable with $E_{\frac{1}{2}}$ = 298 mV.[44]

pH Measurements

Measurements were made using a Radiometer, PHM 84 equipped with a saturated calomel combined electrode. Standardizations were made just prior to measurements using pH 7.00 and pH 4.01 buffer solutions supplied through Radiometer.

D. Kinetic Methods

Description of the Kinetic Experiment

A stock solution of the binuclear complex to be investigated was first prepared. This stock solution consists of binuclear complex, (3×10^{-4} M), 0.02 M in 4-morpholineethanesulfonic acid (MES), (which gives a pH near 4), and the ionic strength was adjusted to 0.1 M with sodium tosylate (NapTs). The same stock solution was used throughout the series of kinetic investigations for each particular binuclear complex.

Various size cells were used which determined the volume of stock solution pipetted into the cell. The cells were closed with rubber septa, fastened tightly with copper wire, and transferred to the thermostated cell compartment of the spectrophotometer. While each cell was thermostated, argon was supplied (by a line equipped with a chromous bubbler), through one septum needle and vented by another. The purging was continued for 45 minutes, after which time the bleeder needle was first withdrawn, followed immediately by the imput needle. Immediately after the withdraw of both needles, the septa were coated with Lubriseal.

Kinetic runs were initiated after each cell had equilibrated. Twenty minutes from initiating the Eu^{2+} generation, the reductant was ready for injection into the thermostated cell. A gas tight syringe was first purged of air by withdrawing the atmosphere within the erylenmeyer bubbler and injecting it outside the flask. This procedure was repeated eight times. The syringe was dipped into the solution and filled with a quarter volume of liquid. Bubbles were purged from the syringe and the solution was discarded. This procedure was repeated once more. The third sample was adjusted to the desired volume and the

reactions were initiated with this addition.

Once an injection has been made, the time was recorded. The cell was immediately removed from the thermostated compartment by holding the rubber septum portion of the cell system. This was transferred to a vortex mixer briefly and replaced back into the compartment within 5 seconds. The time difference between injections and absorbance readings were then recorded.

Multiple runs in which temperature dependence was investigated, were performed on the Beckman DU-8 spectrophotometer. Absorbance readings were at programed intervals. Data from the Cary came from a continuous curve.

Treatment of Data

The reaction sequence for intramolecular electron transfer fits the scheme:

$$A + B \xrightarrow{\text{fast}} C + D \qquad (18)$$

$$C \xrightarrow{\text{slow}} E \qquad (19)$$

$$E \xrightarrow{\text{fast}} F + G \qquad (20)$$

In this sequence, A = $(pic)(NH_3)_4Ru(III)(NH_2\text{-}R\text{-}NH_2)Co(III)(NH_3)_4(H_2O)$, B = Eu^{2+}, C = $(pic)(NH_3)_4Ru(II)(NH_2\text{-}R\text{-}NH_2)Co(III)(NH_3)_4(H_2O)$, D = Eu^{3+}, E = $(pic)(NH_3)_4Ru(III)(NH_2\text{-}R\text{-}NH_2)Co(II)(NH_3)_4(H_2O)$, F = $(pic)(NH_3)_4Ru(III)(NH_2\text{-}R\text{-}NH_2)$, and G = Co(II)(aq).

The first reaction, (18), has been demonstrated for systems involving Eu^{2+} reduction of $Ru(III)(NH_3)_5(py)^{3+}$ at 1 M ClO_4^- to have a rate constant of 5.4×10^4 $M^{-1}s^{-1}$.[45] The last reaction in the series is essentially diffusion controlled.[46] The rate should therefore be dependent on the second step, which is observed by following the decrease of the ruthenium-picoline metal to ligand charge transfer (MLCT)

band at 388 nm. The following relationship should result:

$$-\frac{d[Ru(II)]}{dt} = k_{et}[Ru(II)] \tag{21}$$

$$-\int_{c_o}^{c}\frac{d[Ru(II)]}{[Ru(II)]} = k_{et}\int_{o}^{t}dt \tag{22}$$

$$-\ln[Ru(II)]\Big|_{c_o}^{c} = k_{et}t\Big|_{o}^{t} \tag{23}$$

$$\ln c_o - \ln c = k_{et}t \tag{24}$$

Apparent rate constants were first calculated from plots of $\ln\frac{(OD_t - OD_\infty)}{(OD_o - OD_\infty)}$ vs t which was used to give initial slopes equal to k_{et}. Equation (24) was then treated to give the nonlinear least squares function:

$$\ln(OD_o - OD_\infty) - \ln(OD_t - OD_\infty) = k_{et}t \tag{25}$$

$$\frac{(OD_t - OD_\infty)}{(OD_o - OD_\infty)} = e^{-k_{et}t} \tag{26}$$

$$OD_t = OD_\infty + (OD_o - OD_\infty)e^{-k_{et}t} \tag{27}$$

The data were entered into the Prophet system to fit the function shown in equation (27) to five half lives.

For an intermolecular electron transfer, there are two possible pathways which exist:

$$2A + 2B \xrightarrow{\text{fast}} 2C + 2D \tag{28}$$

$$2C \xrightarrow{\text{slow}} C' + C'' \xrightarrow{\text{fast}} F + G \quad (2C \xrightarrow{\text{slow}} 2E) \tag{29}$$

Here the two new species C' = $(pic)(NH_3)_4Ru(II)(NH_2\text{-}R\text{-}NH_2)Co(II)(NH_3)_4(H_2O)$ and C'' = $(pic)(NH_3)_4Ru(III)(NH_2\text{-}R\text{-}NH_2)Co(III)(NH_3)_4(H_2O)$. The likelyhood of products formed by going through E seems highly improbable. In this treatment, C' and C'' are further reacting species, C' with its Ru(II) center and C'' with its Co(III) center. For such consiterations just mentioned the condition of [Ru(II)] = [Co(III)] will

prevail, giving the general rate equations:

$$-\frac{d[Ru(II)]}{dt} = k_{et}[Ru(II)]^2 \tag{30}$$

$$-\frac{d[Ru(II)]}{[Ru(II)]^2} = k_{et}dt \tag{31}$$

$$-\int_{c_o}^{c}\frac{d[Ru(II)]}{[Ru(II)]^2} = k_{et}\int_{o}^{t}dt \tag{32}$$

$$\frac{1}{[Ru(II)]}\Big|_{c_o}^{c} = k_{et}t\Big|_{o}^{t} \tag{33}$$

$$\frac{1}{c} - \frac{1}{c_o} = k_{et}t \tag{34}$$

Apparent rate constants were again found by plotting $1/\frac{(OD_t - OD_\infty)}{(OD_o - OD_\infty)}$ vs t, from which the intercept at 2 x $[Ru^{2+}] = k_{et}$. Equation (34) can then be treated to give the nonlinear least squares function:

$$\frac{\varepsilon b}{(OD_t - OD_\infty)} - \frac{\varepsilon b}{(OD_o - OD_\infty)} = k_{et}t \tag{35}$$

$$\frac{1}{(OD_t - OD_\infty)} = k't + \frac{1}{(OD_o - OD_\infty)} \tag{36}$$

$$\frac{1}{(OD_t - OD_\infty)} = \frac{k'tOD_o - k'tOD_\infty + 1}{(OD_o - OD_\infty)} \tag{37}$$

$$(OD_t - OD_\infty) = \frac{(OD_o - OD_\infty)}{k'tOD_o - k'tOD_\infty + 1} \tag{38}$$

$$OD_t = \frac{(OD_o - OD_\infty)}{k'tOD_o - k'tOD_\infty + 1} + OD_\infty \tag{39}$$

Once the value for k' has been minimized then $k_{et} = k'\varepsilon b$, where ε is the extinction coeffcient for the particular complex investigated, and b is the path length of the particular cell used. Absorbances were used only for the concentrations which apply to the intermolecular electron transfer process, which may be determined by dilution experiments. These experiments are further explained in Chapter 3.

Activation Parameters

The enthalpy of activation, $\Delta H^{\ddagger}$, was calculated from the slope obtained from the Eyring plot of ln(k/T) vs. (1/T), where the slope = $-\Delta H^{\ddagger}/R$.[10] The entropy of activation, $\Delta S^{\ddagger}$, was calculated from the standard treatment of absolute rate theory:[11]

$$\Delta S^{\ddagger} = R[\ln k_{298} - \ln \nu] + \Delta H^{\ddagger}/298 \qquad (40a)$$

Where

$$\nu = k_B T/h = 6.2 \times 10^{12} \text{ at } T = 298°K \qquad (40b)$$

A linear least squares program was used from the Prophet system to calculate $\Delta H^{\ddagger}$ values.

CHAPTER 3

RESULTS

A. Electron Transfers with $[(pic)(NH_3)_4Ru(3,7dac)Co(NH_3)_4(H_2O)^{6+}$

When a 90% stiochometric addition of Eu^{2+} is made to a cell containing the binuclear complex, an immediate yellow color develops. This color is attributable to the Ru(II) ligand charge transfer band. Once reduced, the ruthenium site may undergo electron transfer by either the intermolecular route, which is favored at higher concentrations, or by the intramolecular route. To test this behavor, the kinetics for a dilution series were studied at 25.0°C. There was an initial change in the observed rate constant after the first dilution, from 3×10^{-4} M to 1.5×10^{-4} M, after which further dilutions no longer affected the observed rate constant. Figure 10 illustrates this effect with concentration and rate dependence. Table IX shows the rate constants obtained from this series of dilutions.

Runs to determine the temperature dependence of the reaction rate were made from the same 3×10^{-4} M stock by diluting 10 ml of this stock to 100 ml. All dilutions mentioned above were made with the same 0.08 M NapTs - 0.02 M MES solution. Two ranges are studied in this series. One range was studied from 25°C to 15°C. These results are shown in Figure 11 and Table X. The other range was studied from 30°C to 45°C. These results are shown in Figure 12 and Table XI.

Periodically, solutions were monitored for the formation of Co^{2+} after the reaction had reached completion. These cobalt concentrations were obtained spectrophotometrically by the potassium thiocynate-acetonitrile method described previously. In all cases where an analysis had been run, the $[Co^{2+}]$ was equal to the amount of Eu^{2+}

Figure 10. Plots of Concentration Dependence of k_{et} for $[(pic)(NH_3)_4Ru(3,7dac)Co(NH_3)_4(H_2O)]^{5+}$.

Concentrations are symbolized as follows:

+ 1.1×10^{-5} M

□ 3.2×10^{-5} M

* 7.1×10^{-5} M

○ 2.1×10^{-4} M

A. This is a plot of $\log(OD_t - OD_\infty)/(OD_o - OD_\infty)$ vs time in seconds.

B. This is a plot of $(OD_t - OD_\infty)/ (OD_o - OD_\infty)$ vs time in seconds.

The Y axis in both A and B represent the percentage of reaction progress where 0.0 on A, and 1.0 on B represent 100% [Ru(II)].

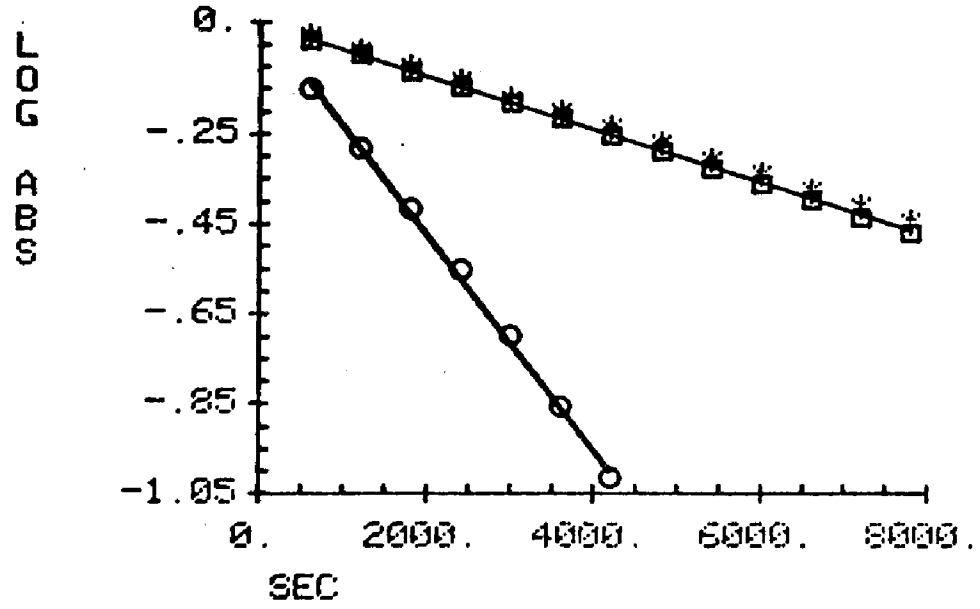
LOG ABS
0.
-.25
-.45
-.65
-.85
-1.05
0.
2000.
4000.
6000.
8000.
SEC

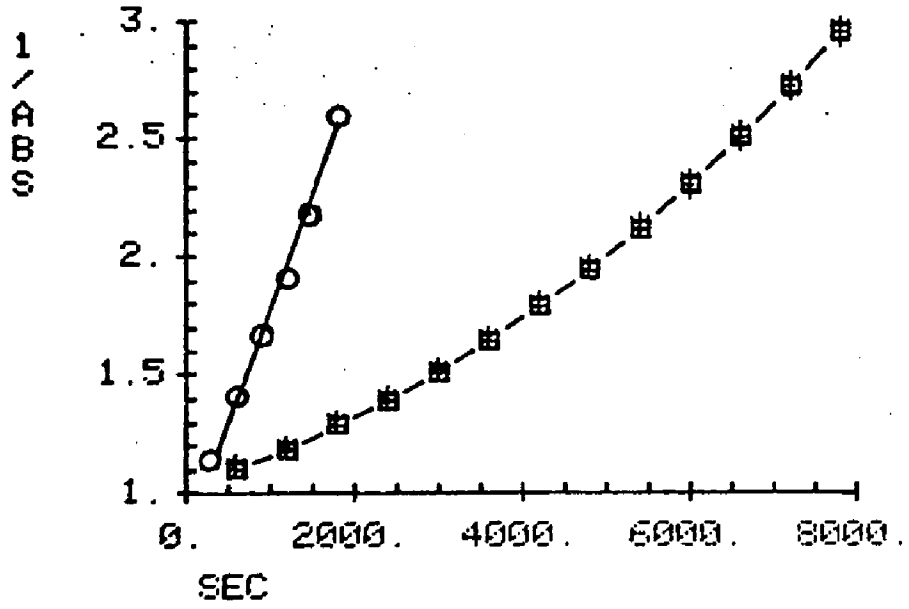
1/ABS
3.
2.5
2.
1.5
1.
0.
2000.
4000.
6000.
8000.
SEC

C. This plot represents 95% of the reaction as 1/concentration vs time. The dotted line depicts the linear portion shown in plot B (which is linear to nearly three half lives). If this reaction were second order throughout the entire experiment, all points would lie on this line. These points are plotted from a continuous curve at 10 minute intervals.

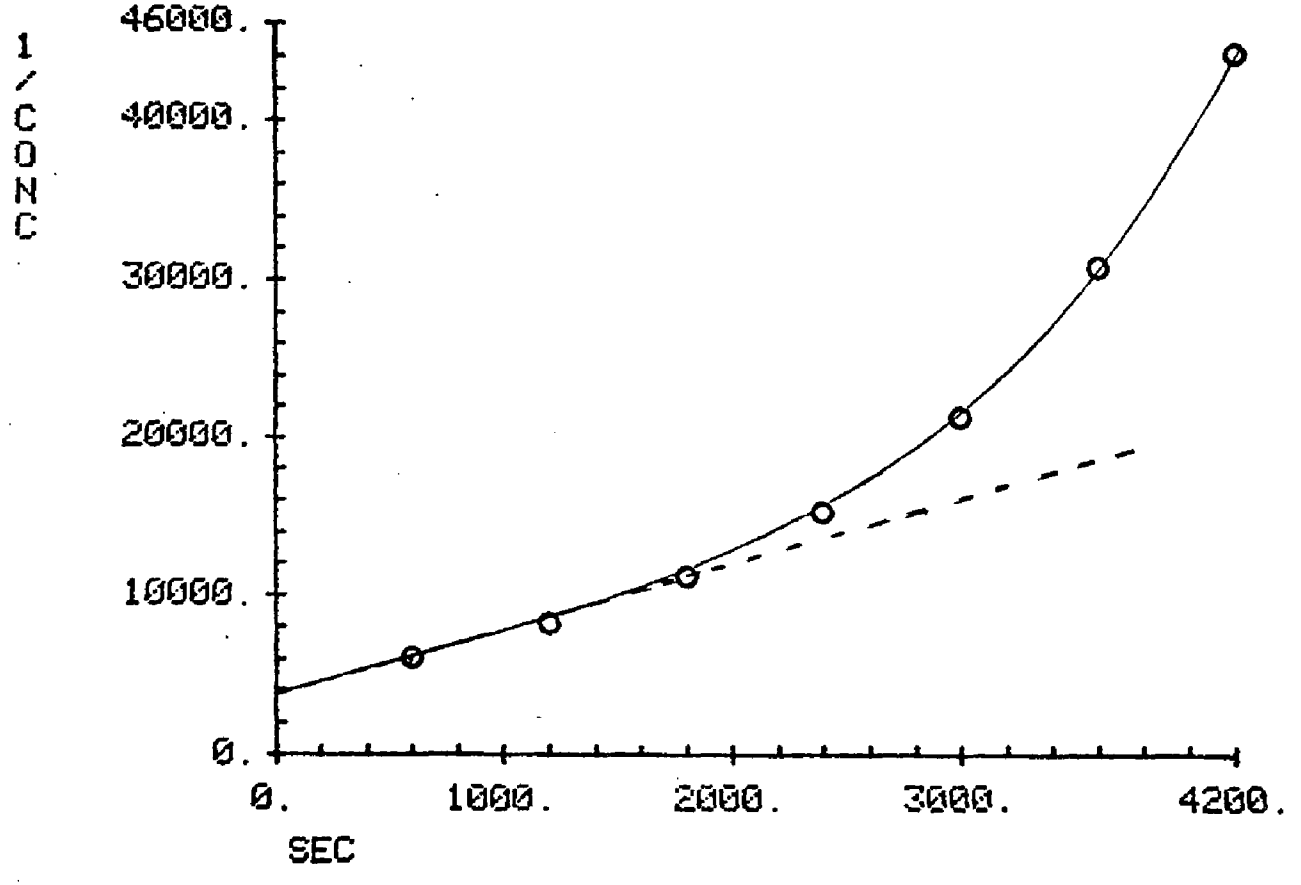
1/CONC
46000.
40000.
30000.
20000.
10000.
0.
0.
1000.
2000.
3000.
4200.
SEC

Table IX. Effects of Concentration on k_{et} for $[(pic)(NH_3)_4Ru(3,7dac)Co(NH_3)_4(H_2O)]^{5+}$.

$[Ru^{2+}] \times 10^4$ (M)	$k_{et} \times 10^4$ (s^{-1})	k_{et} ($M^{-1}s^{-1}$)
2.1	5.39	4.2[a]
0.71	1.36	-
0.32	1.45	-
0.11	1.28	-

The pH = 4.0 with 0.02 M MES and 0.08 M NapTs. All of these kinetic runs were studied at 25.0°C.

[a]Calculated from the linear fit of the plot in Figure 10-B at 2.1×10^{-4} M.

Figure 11. Eyring Plot of Temperature Dependence for $[(pic)(NH_3)_4Ru(3,7dac)Co(NH_3)_4(H_2O)]^{5+}$ For Intramolecular Electron Transfer (First Order).

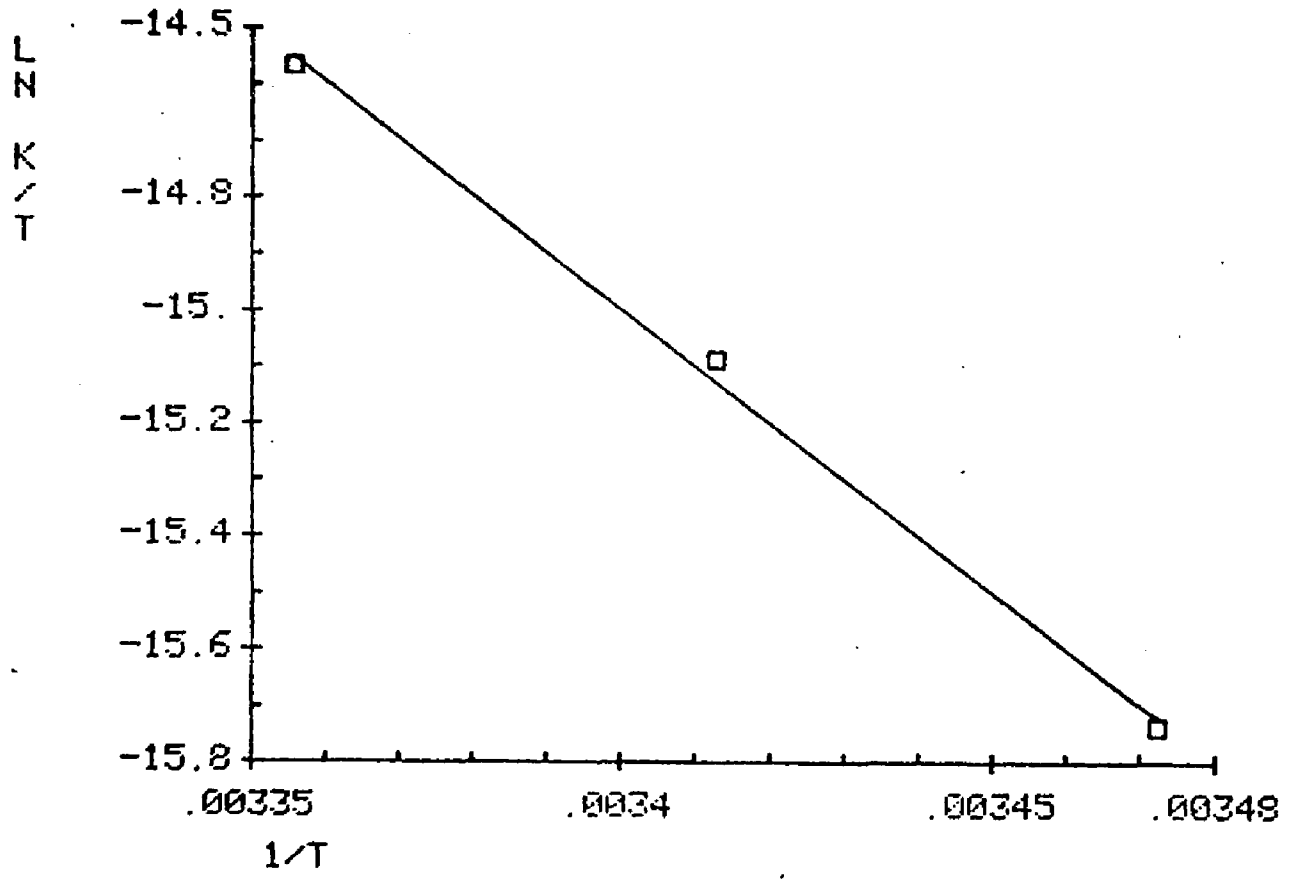
LN K/T
-14.5
-14.8
-15.
-15.2
-15.4
-15.6
-15.8
.00335
.0034
.00345
.00348
1/T

Table X. First Order Temperature Dependence for $[(pic)(NH_3)_4Ru(3,7dac)Co(NH_3)_4(H_2O)]^{5+}$.[a]

T°C	$[Ru^{2+}] \times 10^5$ M	$k_{et} \times 10^4$ s^{-1}
15.0	3.2	0.482
	2.8	0.369
20.0	3.0	0.856
	2.5	0.785
25.0	7.1	1.36
	3.2	1.45

[a]Data are for replicate runs.

The pH = 4.0 with 0.02 M MES and 0.08 M NapTs.

$\Delta H^{\ddagger}$ = 21.0 ± 1.3 kcal/mole

$\Delta S^{\ddagger}$ = -5.6 ± 0.3 cal/mole·°K

Figure 12. Eyring Plot of Temperature Dependence for $[(pic)(NH_3)_4Ru(3,7dac)Co(NH_3)_4(H_2O)^{5+}$ For Intermolecular Electron Transfer (Second Order).

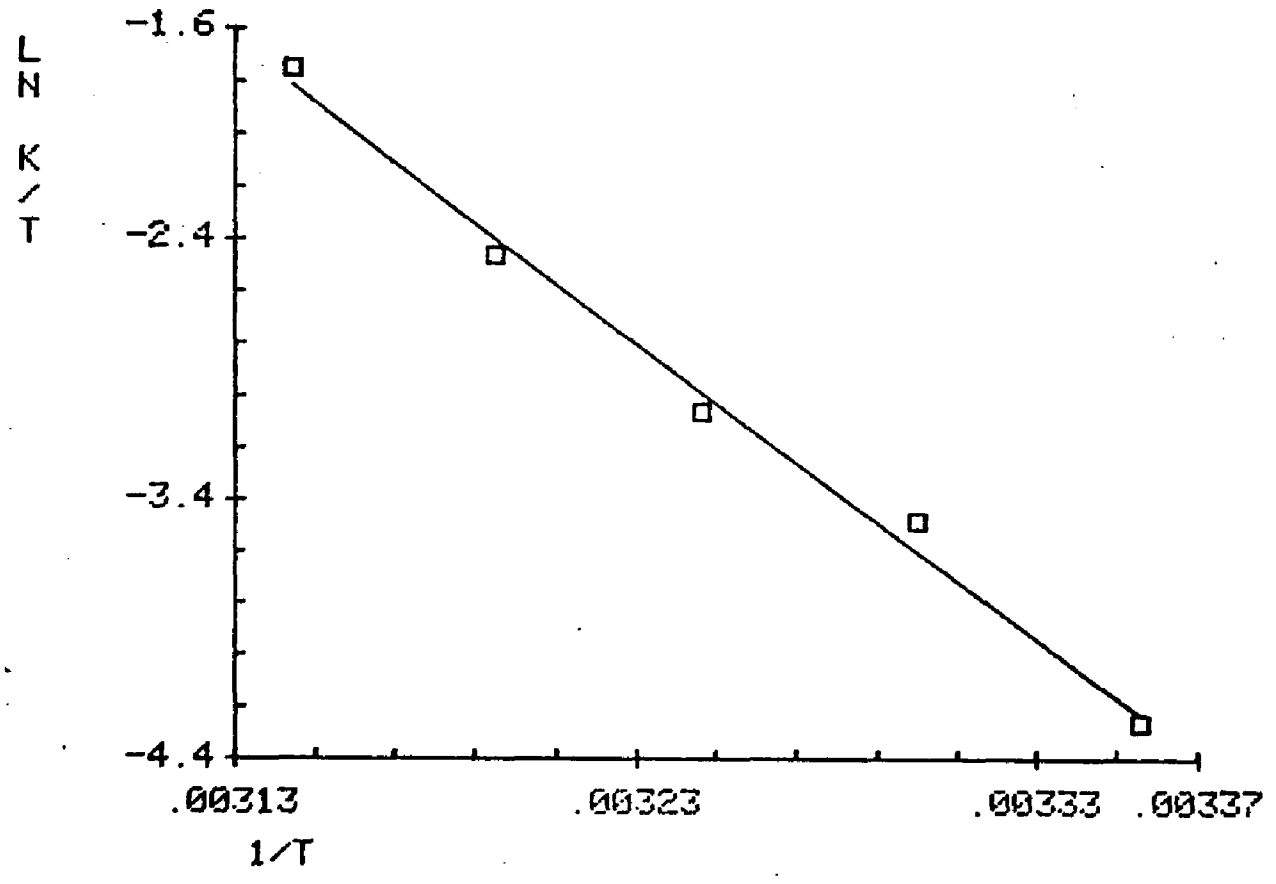
LN K/T
-1.6
-2.4
-3.4
-4.4
.00313
.00323
.00333
.00337
1/T

Table XI. Second Order Temperature Dependence for $[(pic)(NH_3)_4Ru(3,7dac)Co(NH_3)_4(H_2O)]^{5+}$.

T°C	$[Ru^{2+}]$ x 10^4 M	k_{et} $M^{-1}s^{-1}$
25.0	2.1	4.2
30.0	1.8	9.31
35.0	3.0	15.1[a]
	3.1	13.7[a]
40.0	2.6	26.6[a]
	2.7	26.7[a]
45.0	2.5	55.0

[a]Duplicate runs.

The pH = 4.0 with 0.02 M MES and 0.08 M NapTs.

$\Delta H^{\ddagger}$ = 22.7 ± 0.9 kcal/mole

$\Delta S^{\ddagger}$ = 20.5 ± 0.9 cal/mole·°K

injected into the cell, which was about 90% of the total binuclear complex species.

Measurements were made after every kinetic run to check for any pH change after the reaction had reached completion. The pH, in most cases, was found to be within 0.1 pH units of the initial stock solution at 4.0.

A test for oxygen leakage was also run on the $Ru(NH_3)_4(pic)(3,7dac)^{4+}$ complex. A solution was prepared under the same buffer and ionic strength conditions, with the $[Ru^{3+}]$ determined to be at 9.7×10^{-5} M spectrophotometrically. The amount of $[Ru^{2+}]$ generated by Eu^{2+} addition was 6.5×10^{-5} M. This run was monitored at 25°C for 750 minutes. Extrapolation of the linear log plot of $(OD_t - OD_\infty)/(OD_o - OD_\infty)$ to 0.5 gives the $k_{obs} = 5.0 \times 10^{-6}$ s^{-1} by the half life method. Under these conditions, the rate of Ru(II) oxidation due to oxygen leakage is approximately 50 times less than the electron transfer reaction of the binuclear experiment.

B. Electron Transfers with $[(pic)(NH_3)_4Ru(3,17daa)Co(NH_3)_4(H_2O)]^{6+}$

Rates of electron transfer for a series of successively less concentrated solutions were first investigated to determine whether electron transfer was inter- or intramolecular. These runs were performed under the same conditions as with the 3,7dac analog, at 25°C and 0.08 M NapTs and 0.02 M MES. The pH changes were once again found to be in the same range as with the 3,7dac analog: only 0.1 pH unit from the stock solution pH of 4.0. Preparations of successive experiments in the dilution series were handled in the same manner as in the 3,7dac analog experiments. Results from these studies are shown in Figure 13 and Table XII.

Figure 13. Plots of Concentration Dependence of k_{et} for $[(pic)(NH_3)_4Ru(3,17daa)Co(NH_3)_4(H_2O)]^{5+}$.

Concentrations are symbolized as follows:

+ 2.4×10^{-5}

□ 6.8×10^{-5}

* 1.2×10^{-4}

○ 2.4×10^{-4}

A. This is a plot of $\log(OD_t - OD_\infty)/(OD_o - OD_\infty)$ vs time in seconds.

B. This is a plot of $(OD_t - OD_\infty)/(OD_o - OD_\infty)$ vs time in seconds.

The Y axis in both A and B represent the percentage of reaction progress where 0.0 on A, and 1.0 on B represent 100% [Ru(II)].

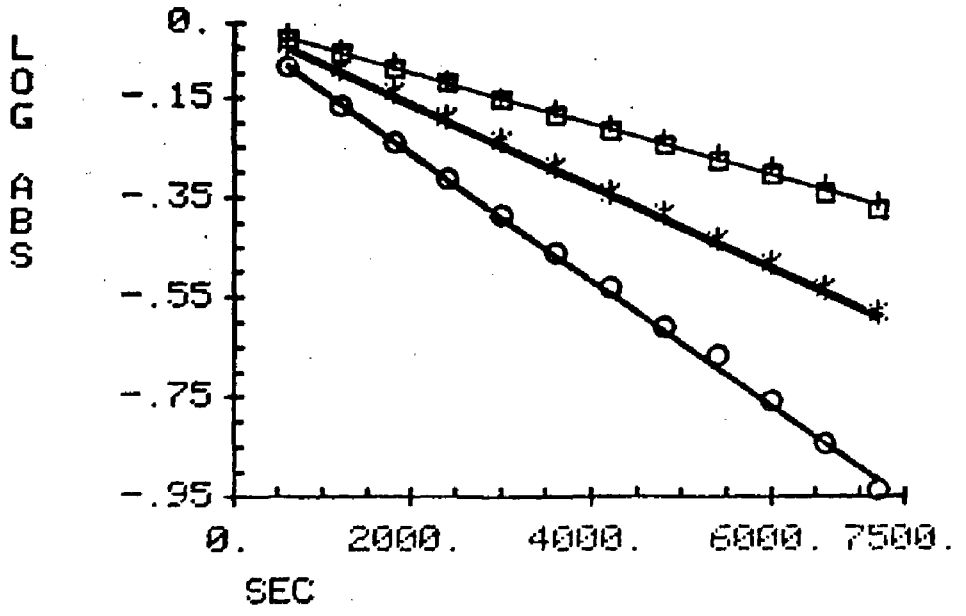
LOG ABS
0.
-.15
-.35
-.55
-.75
-.95
0.
2000.
4000.
6000.
7500.
SEC

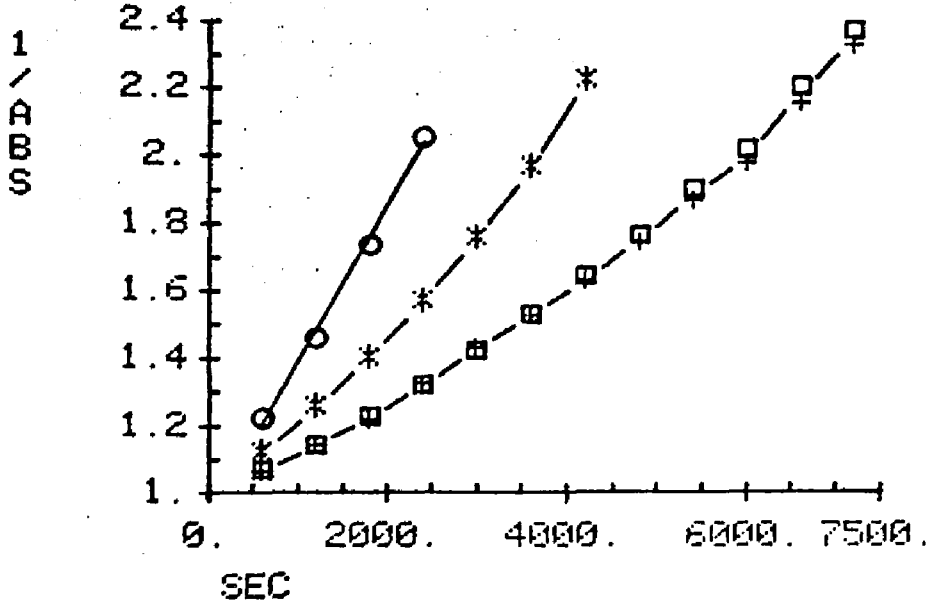
1/ABS
2.4
2.2
2.
1.8
1.6
1.4
1.2
1.
0.
2000.
4000.
6000.
7500.
SEC

C. This plot represents 95% of the reaction as 1/concentration vs time. The dotted line depicts the linear portion shown in plot B (which is linear to nearly three half lives). If this reaction were second order throughout the entire experiment, all points would lie on this line. These points are plotted from a continuous curve at 10 minute intervals.

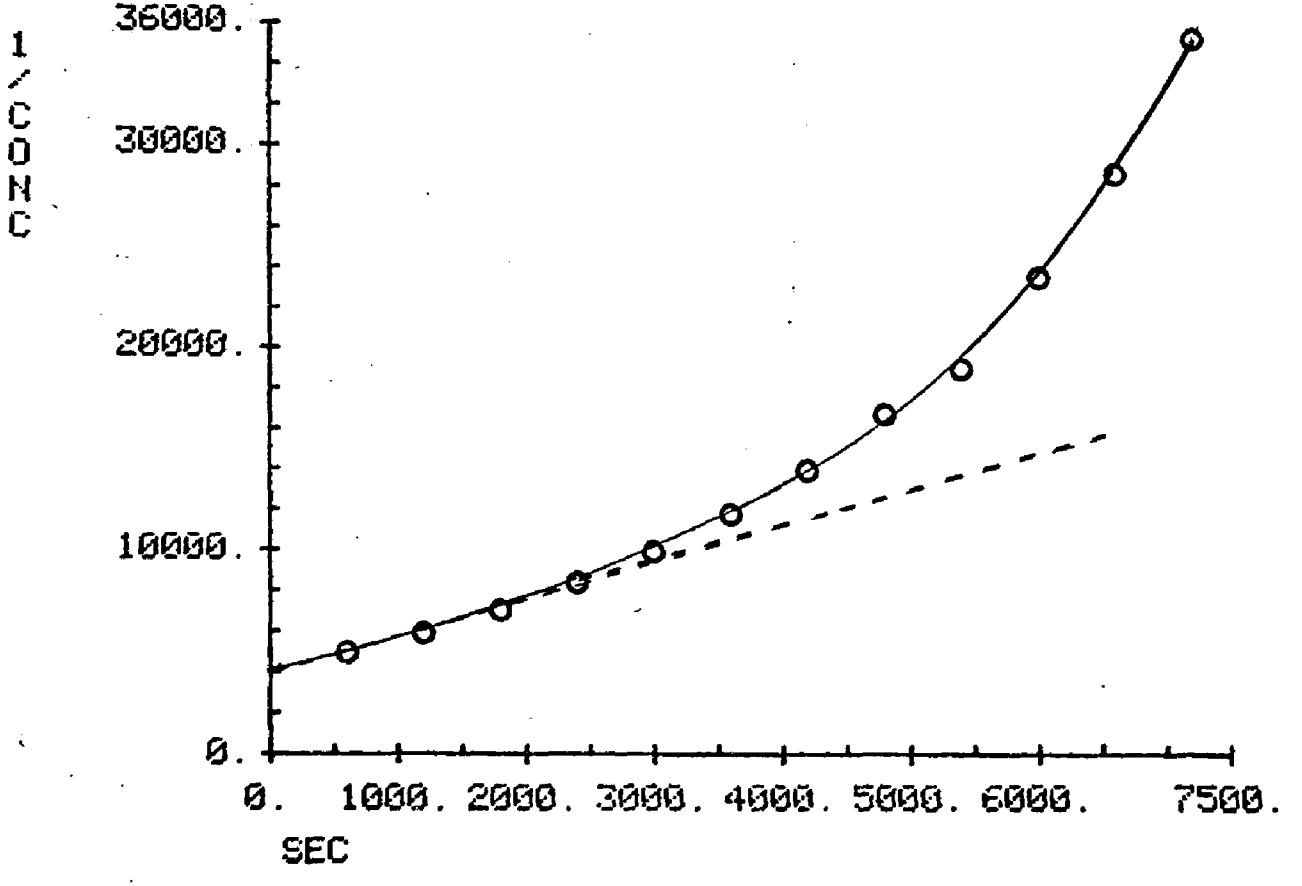
1/CONC
36000.
30000.
20000.
10000.
0.
0. 1000. 2000. 3000. 4000. 5000. 6000. 7500.
SEC

Table XII. Effects of Concentration on k_{et} for $[(pic)(NH_3)_4Ru(3,17daa)Co(NH_3)_4(H_2O)]^{5+}$.

$[Ru^{2+}] \times 10^4$ (M)	$k_{et} \times 10^4$ (s^{-1})	k_{et} ($M^{-1}s^{-1}$)
2.4	3.02	1.9[a]
1.2	1.87	-
0.68	1.31	-
0.24	1.14	-

The pH = 4.0 with 0.02 M MES and 0.08 M NapTs. All of these kinetic runs were studied at 25.0°C.

[a]Calculated from the linear fit of the plot in Figure 13-B at 2.1×10^{-4} M.

Temperature dependence was investigated for the intramolecular electron transfer from 30°C to 20°C. The [Ru^{2+}] concentration chosen for these experiments was 5 x 10^{-5} M. Data obtained from these experiments are shown in Figure 14 and Table XIII.

An experiment was performed at this point to show that once all the cobalt has been reduced to Co^{2+}, the charge transfer band of the Ru^{2+} could be regenerated and its decrease should only be due to the presence of oxygen. To demonstrate this, after the first run at 20°C had reached completion, Eu^{2+} was injected into the cell to regenerate the charge transfer band at 388 nm. Further injections of Eu^{2+} were made until the absorbance at 388 nm remained constant. This solution was then placed in the dark for 24 hours.

Twenty four hours after the conversion of all Ru^{3+} to Ru^{2+}, the cell was once again placed into the spectrophotometer at 20°C. The initial absorbance reading had decreased from the saturated level recorded 24 hours before. The cell was left in the spectrophotometer and the decrease in the charge transfer was followed for 70 minutes. Again a linear log plot of $(OD_t - OD_\infty)/(OD_o - OD_\infty)$ gives an extrapolated k_{obs} similar to that seen for the $[Ru(NH_3)_4(pic)(3,7dac)]^{4+}$ measured previously. This result not only indicates the same oxygen leakage rate, but also indicates a reaction which is different from that initially seen with intact binuclear sample when the Eu^{2+} is first injected.

In one of the duplicate runs at 30°C, $Ru(NH_3)_6^{2+}$ was used as the reducing agent for the reaction series. A nearly identical rate is seen when Eu^{2+} is used as the reductant under the same conditions. This experiment further supports the mechanism whereby the initial binuclear

Figure 14. Eyring Plot of Temperature Dependence for $[(pic)(NH_3)_4Ru(3,17daa)Co(NH_3)_4(H_2O)]^{5+}$ For Intramolecular Electron Transfer (First Order).

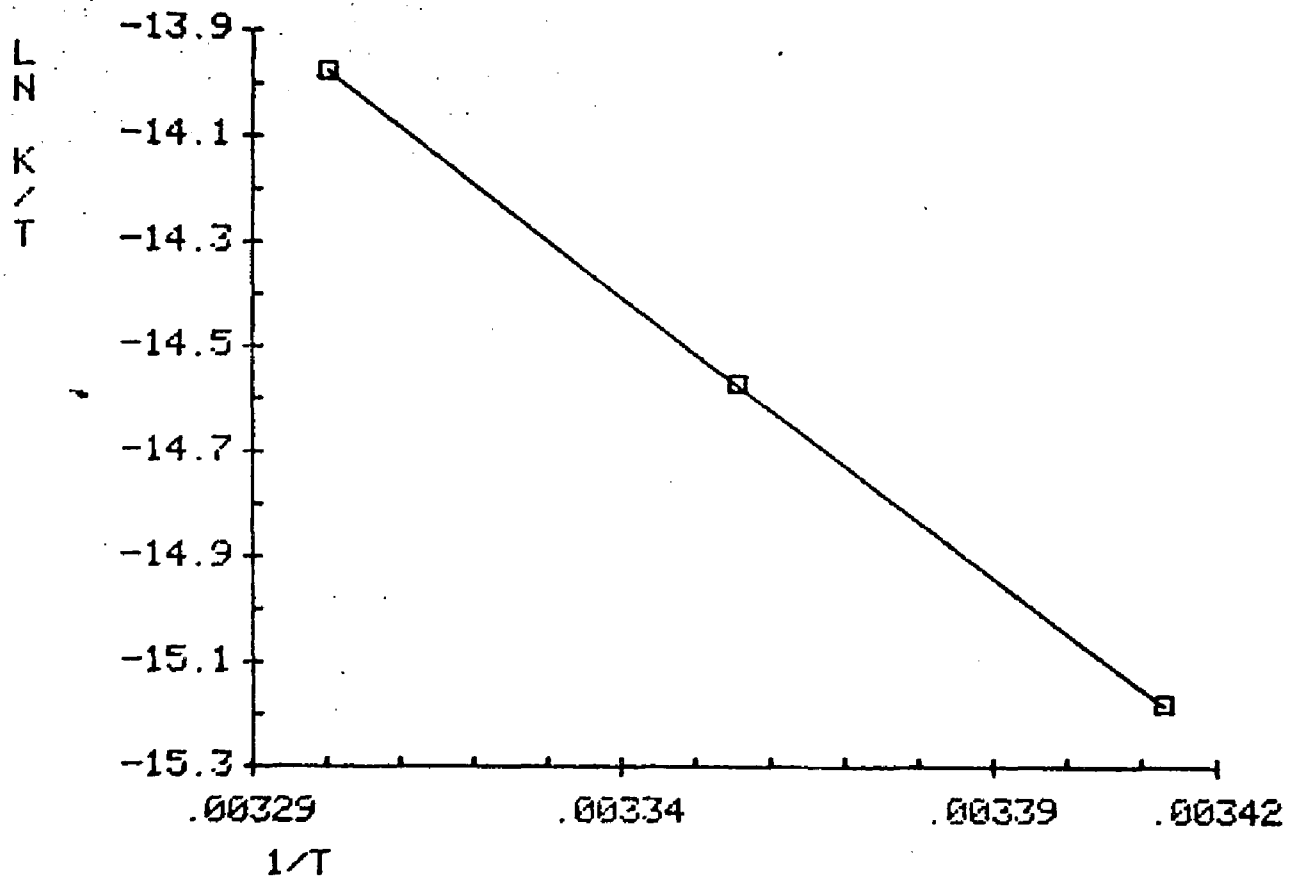
LN K/T
-13.9
-14.1
-14.3
-14.5
-14.7
-14.9
-15.1
-15.3
.00329
.00334
.00339
.00342
1/T

Table XIII. First Order Temperature Dependence for $[(pic)(NH_3)_4Ru(3,17daa)Co(NH_3)_4(H_2O)]^{5+}$.

T°C	$[Ru^{2+}] \times 10^5$ M	$k_{et} \times 10^4$ s^{-1}
20.0	7.8	0.750
25.0	6.8	1.31[a]
	7.7	1.53[a]
30.0	7.4	2.65[a,b]
	6.9	2.51[a]

[a]Data are for replicate runs.

[b]$Ru(NH_3)_6^{2+}$ is used as the reductant.

The pH = 4.0 with 0.02 M MES and 0.08 M NapTs.

$\Delta H^{\ddagger}$ = 21.2 ± 0.1 kcal/mole

$\Delta S^{\ddagger}$ = -5.0 ± 0.1 cal/mole·°K

reduction occurs in a fast step, followed by the Ru(II)→Co(III) electron transfer in the rate determining step.

The intermolecular activation parameters were calculated from studies following electron transfers at 30°C and 40°C. The rate calculated from the dilution experiments described previously was also used in the Eyring plot for second order temperature dependence. These results are shown in Figure 15 and Table XIV.

C. Electron Transfers with $[(pic)(NH_3)_4Ru(pacm)Co(NH_3)_4(H_2O)]^{6+}$

Second order temperature dependence was followed in this series from 30.0°C to 40°C. Stock solutions were prepared similarly as with the steroid cases. Figure 16 is the Eyring plot of this series. Data used for the temperature dependence are shown in Table XV.

Figure 15. Eyring Plot of Temperature Dependence for $[(pic)(NH_3)_4Ru(3,17daa)Co(NH_3)_4(H_2O)]^{5+}$ For Intermolecular Electron Transfer (Second Order).

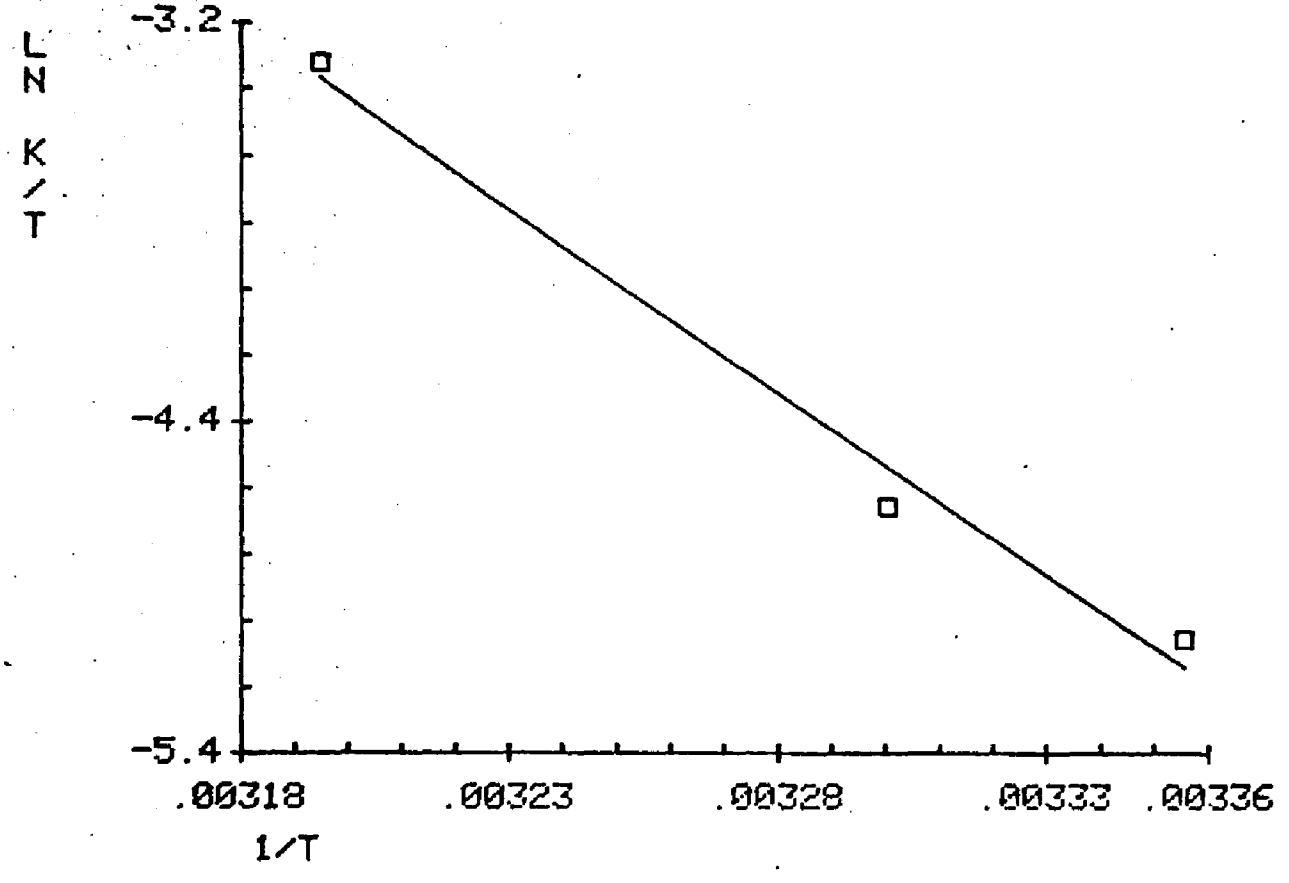
-3.2
-4.4
-5.4
LN K/T
.00318
.00323
.00328
.00333
.00336
1/T

Table XIV. Second Order Temperature Dependence for $[(pic)(NH_3)_4Ru(3,17daa)Co(NH_3)_4(H_2O)]^{5+}$.

T°C	$[Ru^{2+}] \times 10^4$ M	k_{et} $M^{-1}s^{-1}$
25.0	2.4	1.9
30.0	2.2	2.56[a]
	2.0	3.21[a]
40.0	2.3	10.5[a]
	2.6	12.1[a]

[a]Duplicate runs.

The pH = 4.0 with 0.02 MES and 0.08 M NapTs.

$\Delta H^{\ddagger}$ = 21.9 ± 2.3 kcal/mole

$\Delta S^{\ddagger}$ = 16.2 ± 2.2 cal/mole·°K

Figure 16. Eyring Plot of Temperature Dependence for $[(pic)(NH_3)Ru(pacm)Co(NH_3)_4(H_2O)]^{5+}$ For Intermolecular Electron Transfer (Second Order).

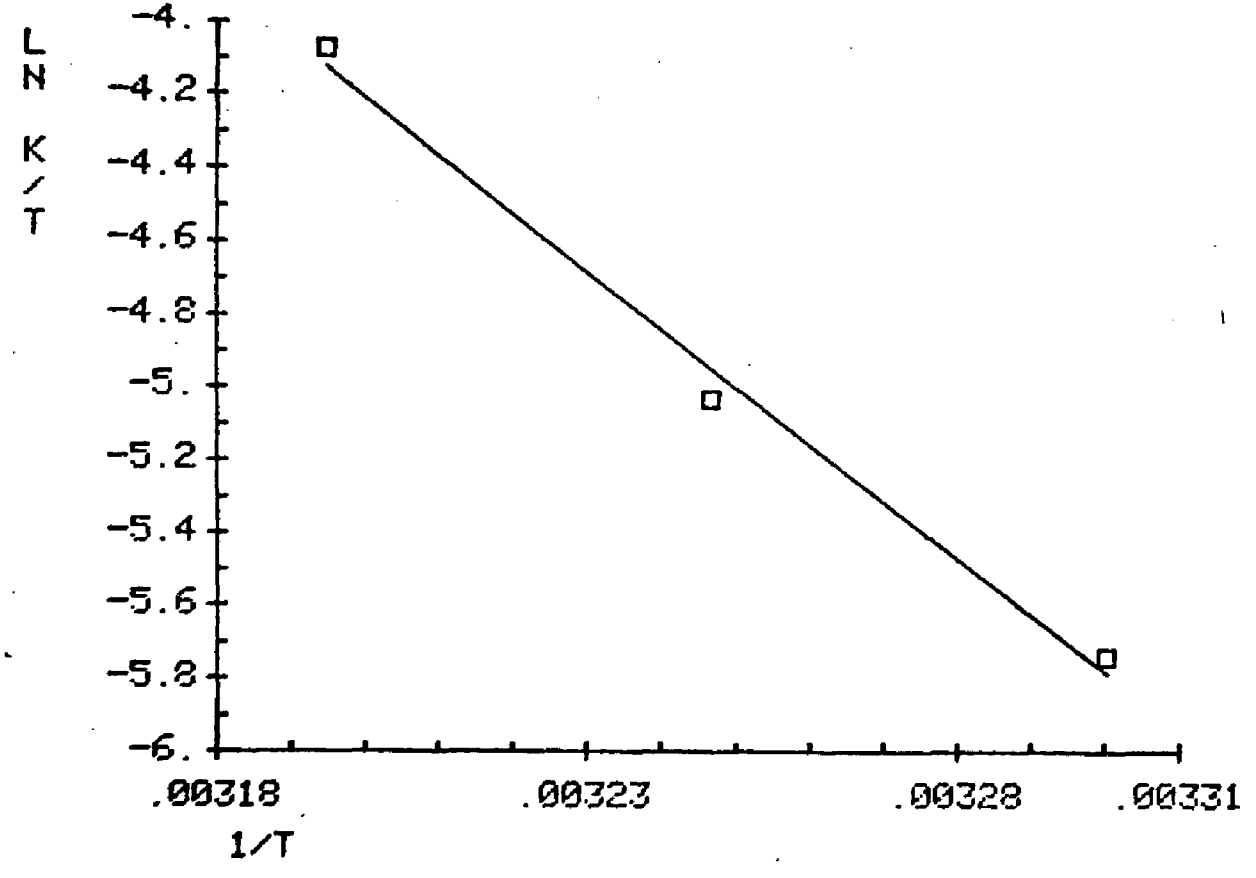
LN K/T
-4.
-4.2
-4.4
-4.6
-4.8
-5.
-5.2
-5.4
-5.6
-5.8
-6.
.00318
.00323
.00328
.00331
1/T

Table XV. Second Order Temperature Dependence for $[(pic)(NH_3)_4Ru(pacm)Co(NH_3)_4(H_2O)]^{5+}$.

T°C	$[Ru^{2+}] \times 10^4$ M	k_{et} $M^{-1}s^{-1}$
30.0	3.0	0.973[a]
	3.0	0.979[a]
	1.6	0.967[a]
35.1	1.4	2.14[a]
	1.6	1.91[a]
40.0	1.4	5.31[a]
	1.3	5.32[a]

[a]Replicate runs.

The pH = 4.0 with 0.02 M MES and 0.08 M NapTs.

$\Delta H^{\ddagger}$ = 31.4 ± 3.0 kcal/ mole

$\Delta S^{\ddagger}$ = 45.0 ± 3.2 cal/mole·°K

CHAPTER 4

DISCUSSION

A. Synthesis

The ultimate goal to any thorough experiment is to meticulously isolate potential troubles, and correct them; leaving no doubt as to the meaning of the results. This project is committed to such an approach and only represents a part of an intricate whole.

An eventual goal of our research in electron transfer reactions is to link a bimetallic complex with a rigid surface to prevent the complication of electron transfer between two separate molecules (intermolecular electron transfer). Before this may be accomplished, it is important to investigate the chemistry of the bimetallic species as free ions in solution. In such a study, convenient and sensitive techniques, such as uv-visible and infrared spectroscopy, cyclic voltammetry, or nuclear magnetic resonance spectrometry may be applied. These measurements provide information for predicting how such molecules will function when bound to a polymeric support.

Silica gels may be readily modified by attachment of pyridine derivatives. These gels are convenient since complexes of ruthenium with pyridine have been well studied.[47,48,49] One purpose of this thesis involves the study of various routes in which a pyridine-ruthenium complex may be used to assemble the entire bimetallic-cholestane system. Picoline was chosen because it closely resembles the ethylpyridyl functionality present on one type of gel which may be used in future studies. Various routes were then designed to test the most effecient method for synthesizing the desired bimetallic complexes.

The most convenient and highest yielding route for synthesizing the bimetallic complex was through the Zn(Hg) amalgam reduction - bromine water oxidation procedure for attaching the cholestane ligand to the tetraaminepicoline ruthenium(III) fragment, (Chapter 2, Section B3 of this thesis). This is by far the most crucial and difficult stage in the synthesis. This is not, however, a convenient route to use for gel attachment. Use of $Ba(CF_3SO_3)_2$ to remove SO_4^{2-} bound to penta-amminepicoline ruthenium(III) would be the most convenient method for silica preparations. Both routes yield the same products, as indicated by similar uv-visible and infrared spectra.

The oxidized and reduced species in homogeneous solution can be differentiated by a shift of the ligand-to-metal charge transfer band in the oxidized state and in the reduced state. In water this change is from 345 nm to 388 nm. A similar shift is observed with the ruthenium-pyridyl system bound to the gel. Here the change (in a cyclohexanone slurry) is from 365 nm to 415 nm. This spectral shift is a strong indication that the ruthenium is covalently bound to a pyridine moiety which is covalently bound to the silica.

Spectral analysis of the cobalt released in the exhaustive reduction of the bimetallic complex bound to silica gel gives a 1:1 ratio of Ru to Co (Table VII). This suggests covalent binding of both the ruthenium and the cobalt. In the cobalt addition stage of the synthesis a severalfold excess of cobalt was used. Adsorption on the silica surface does not, therefore, seem likely.

The adsorption of ionic cobalt complexes onto the silica surface is also precluded by the exhaustive alkylsilylation of the gel previous to metal attachment. In this procedure, a hydrophobic environment is

created at the gel surface. This treatment also enables the synthesis to be carried out in water since the silylated gel does not swell as much as the non-silylated gel. Scheme 1 illustrates the gel preparations.

One other precaution is necessary in this synthesis scheme. The diaminocholanate ester derivative must be reduced to the corresponding alcohol, otherwise the Ru^{3+} reagent undergoes reduction, (presumably to the immino complex through a Shiffs base type reaction).[50,51]

B. Structural Analysis of 3α,7α-diamino-5β-cholestan-24-ol

The stereochemistry of the ligand is important since different epimers would give different metal-to-metal distances in the binuclear complex. High pressure liquid chromatography indicates only one product for the diaminocholestanol.[52] The assignments of the C_3 and C_7 nitrogen positions in this product may be made from the analysis of the proton NMR spectra reported for chenodeoxycholic acid (CDCA) and ursodeoxycholic acid (UDCA), illustrated in Figure 17.[53]

Both CDCA and UDCA have a broad peak between 1.0 and 2.5 ppm. This arises from methylene and methine protons due to extensive spin-spin coupling between protons of similar chemical shift. The epimeric configurational difference between CDCA and UDCA at C_7 causes an altered appearance in the region between 3 to 4 ppm. The $C_7(\beta)$ skeletal proton in CDCA gives rise to a sharp signal at 3.78 ppm, consistent with the Karplus relation for the dihedral angle dependence of the vicinal coupling constant. This downfield shift is further influenced by the steric congestion between the hydroxyl group at C_7 and proton at C_4. The $C_3(\beta)$ proton is assigned at 3.38 ppm.

In UDCA, the methine proton at $C_7(\alpha)$ is coupled strongly to the

Scheme 1

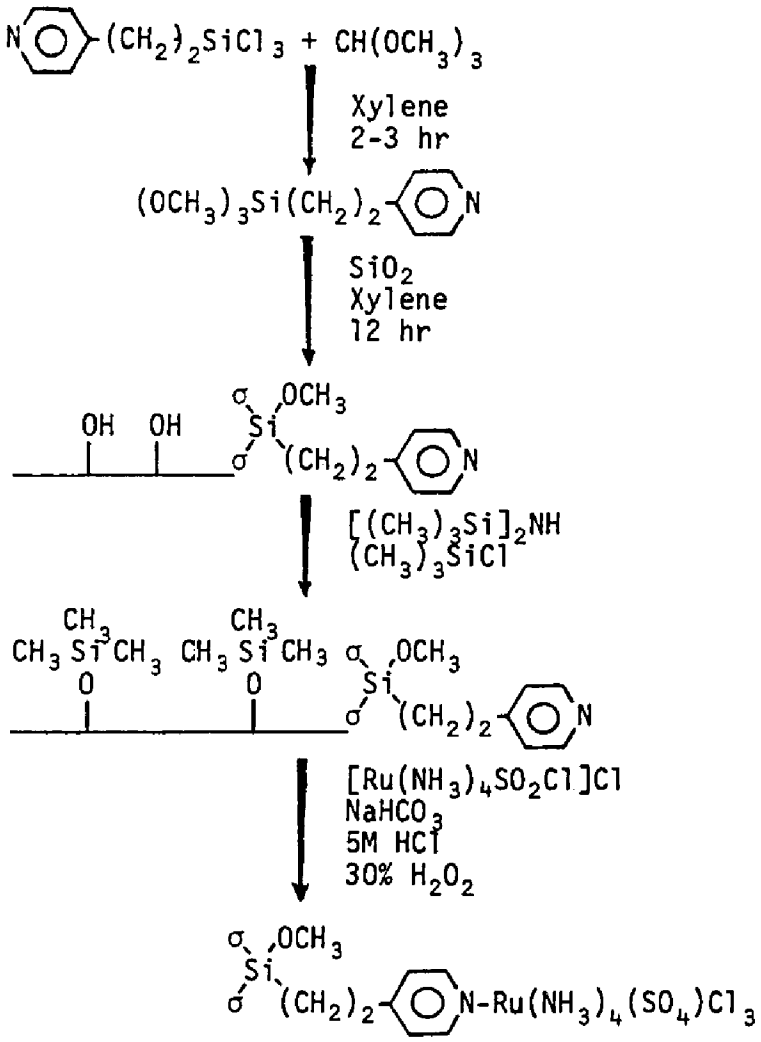
(CH2)2SiCl3 + CH(OCH3)3
Xylene
2-3 hr
(OCH3)3Si(CH2)2
SiO2
Xylene
12 hr
OH OH
OCH3
[(CH3)3Si]2NH
(CH3)3SiCl
[Ru(NH3)4SO2Cl]Cl
NaHCO3
5M HCl
30% H2O2
N-Ru(NH3)4(SO4)Cl3

Figure 17. Proton NMR Spectral Comparisons Between CDCA and UDCA at 25°C. These inserts were taken from the Bagattacharyya and Bankawala article in Analytical Chemistry, Volume 50, Number 11, September 1978.

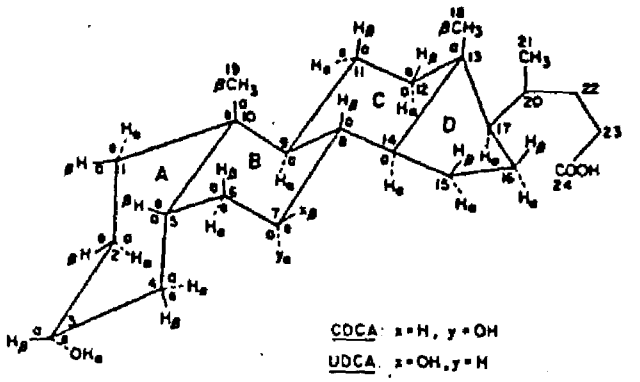

Stereochemical configurations of chenodeoxycholic and ursodeoxycholic acids. The α-bonds are indicated by the dotted lines going behind the plane of the paper, and the β-bonds by the solid lines coming out of the plane of paper. The small letters "a" and "e" refer to "axial" and "equatorial" bonds, respectively

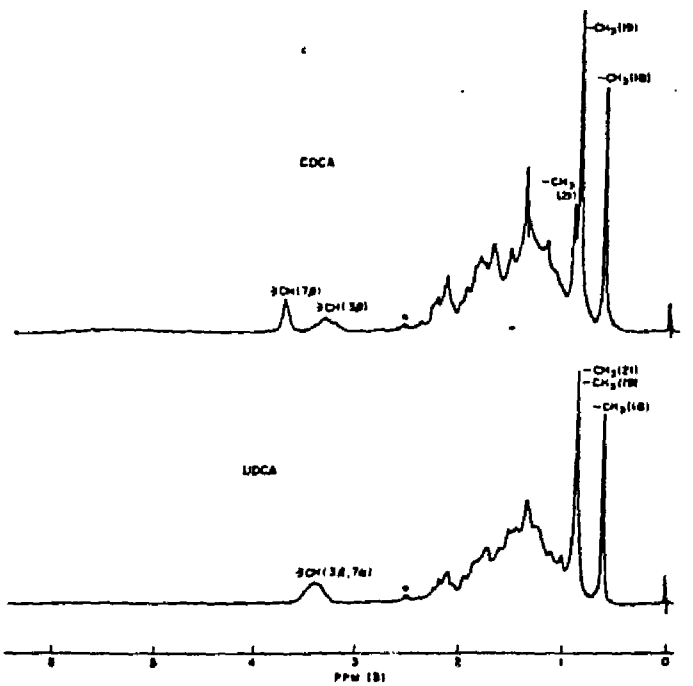

Proton NMR spectra of chenodeoxycholic acid (CDCA) and ursodeoxycholic acid (UDCA) in the mixture of solvents $CDCl_3$ and DMSO-d_6 (8:1 v/v). The solvent peaks are marked with asterisks

axial protons on C_6 and C_8 by virtue of a trans-diaxial relationship. With both $C_7(\alpha)$ and $C_3(\beta)$ being in the axial positions, they are shielded almost equally, so thier resonance positions coincide at 3.45 ppm.

In the proton NMR spectrum of the diaminecholanol (3,7dac), (Figure 18), a sharp signal is seen at 3.58 ppm, and another signal is seen upfield from this at 3.11 ppm. This spectrum is very similar to the CDCA spectrum. The two peaks at 3.11 and 3.58 ppm are slightly upfield from those reported for CDCA, but thier separations are virtually the same (0.47 ppm for 3,7dac and 0.40 ppm for CDCA). From this information, the conformation of 3,7dac is assigned as 3α,7α-diamino-5β-cholestan-24-ol.

Since no crystallographic data are available for the diaminosteroids nor their bimetallic complexes, structural molecules were constructed from known structural parameters of fragments of the molecule. An interactive computer system (Prophet) was used to construct the model.

The structure of 3α,7α-diamino-5β-cholestan-24-ol was derived from cystallographic data for a 3α,7α-dihydroxy derivative, (See Chapter 2. Section C2). Standard N-C bond lengths were used when replacing the hydroxyl oxygens with the amine nitrogens, and the dihedral angles were kept constant. To replace hydroxyl oxygen atoms by amine nitrogen atoms, the coordinates of the trans nitrogen in $Ru(NH_3)_5(pz)^{2+}$ and the cis nitrogen of $Co(NH_3)_5(H_2O)^{3+}$ were used.

Once the bimetallic molecule was assembled on a graphic display terminal, rotations were made about the N_7-C_7, N_3-C_3, N_7-Co, and N_3-Ru bonds until the "optimized" geometry was found. This optimized geometry

Figure 18. Proton NMR Spectrum of 3α,7α-diamino-5β-cholestan-24-ol.

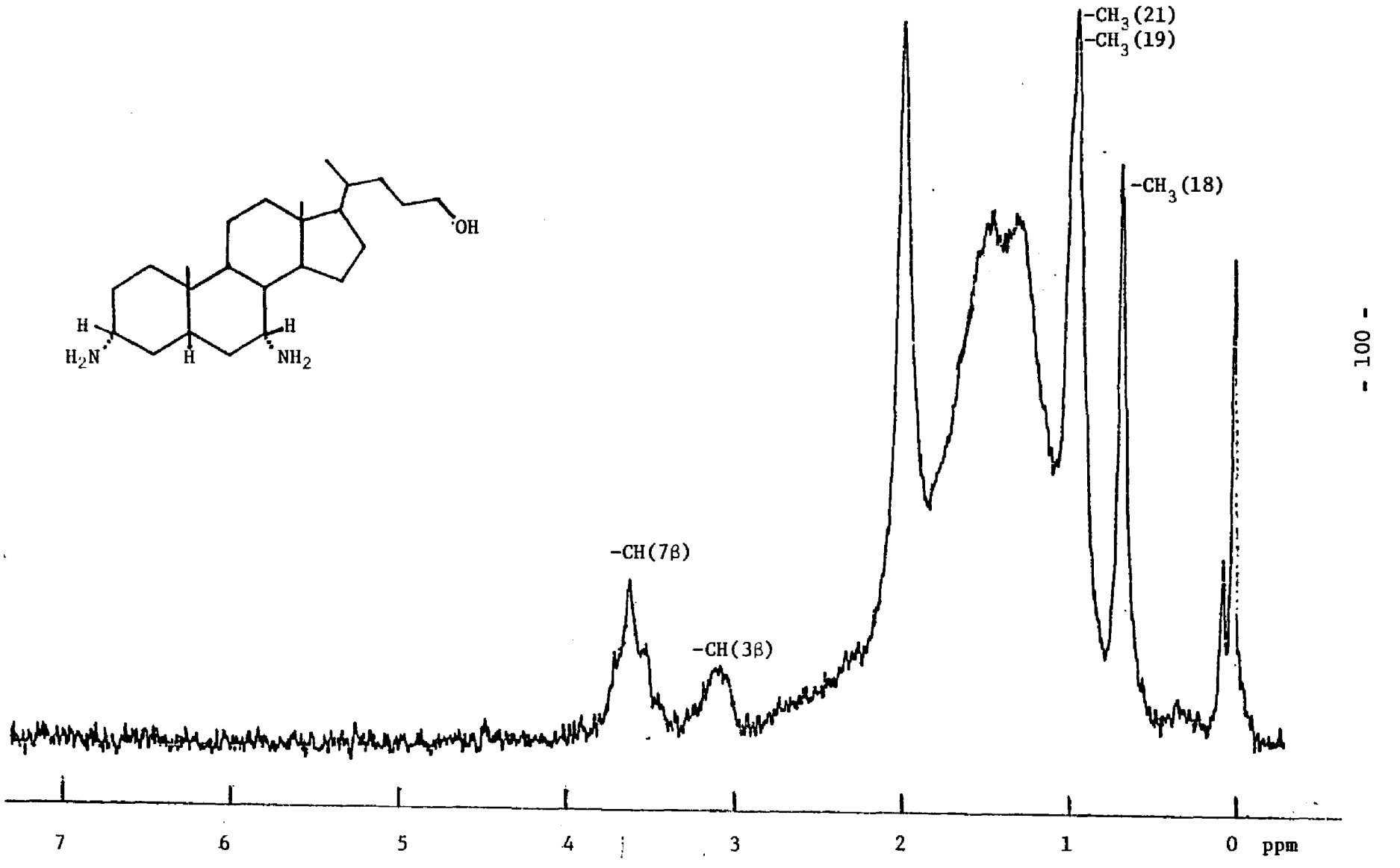
-CH3 (21)
-CH3 (19)
-CH3 (18)
-CH(7β)
-CH(3β)
OH
H
H2N
H
NH2
7
6
5
4
3
2
1
0
ppm

was chosen by moving the metal centers as close as possible, while allowing no approach closer than the van der Waals contact radii of their coordination spheres. The value for the van der Waal radius of hydrogen was chosen as 1.1 Å. The distance separating the cobalt and ruthenium centers was determined to be 7.47 Å. At this distance the metal coordination spheres are nearly touching, with about 0.5 Å separating their coordination spheres, (see Figure 19 for the ORTEP drawing and Figure 20 for a space-filling representation).

One other fine point concluded from the structural analysis is that at the C_7 position of the cobalt attachment, a very constrained environment is observed. Only about 5 degrees of rotation of the C_7- N_7 dihedral of the cobalt coordination sphere result in contact with the cholestane fragment. The C_3 side is more open it this manner. This result is manifested experimentally. In the synthesis of the Ru-diaminocholestanol intermediate by the $Ba(CF_3SO_3)_2$ method, the yellow color of the product (344 nm with ε = 1900) develops within a minute after the ruthenium-complex addition to the methanol medium. When cobalt is first attached to the cholestane, followed by ruthenium addition, the yellow color takes about a half hour to fully develop. It appears that the reaction at one site is slower than at the other site.

C. Structural Analysis of 3β,17β-diamino-5α-androstane

The stereochemical assignment for the 3,17-diaminoandrostane was made using several observations. Various methods of oxime reduction to form amino-androstanes were studied by D.W. Mathieson, et al.[54] Using sodium reduction in alcohol, 89% of the C_3-amine product was β and 95% of the C_{17}-amine product was also β. From this information, the major product for 3,17daa should be $N_3(\beta),N_{17}(\beta)$ about 85%, with about 10%

Figure 19. ORTEP2 Representation of $[(pic)(NH_3)_4Ru(3,7dac)Co(NH_3)_4(H_2O)]^{5+}$.

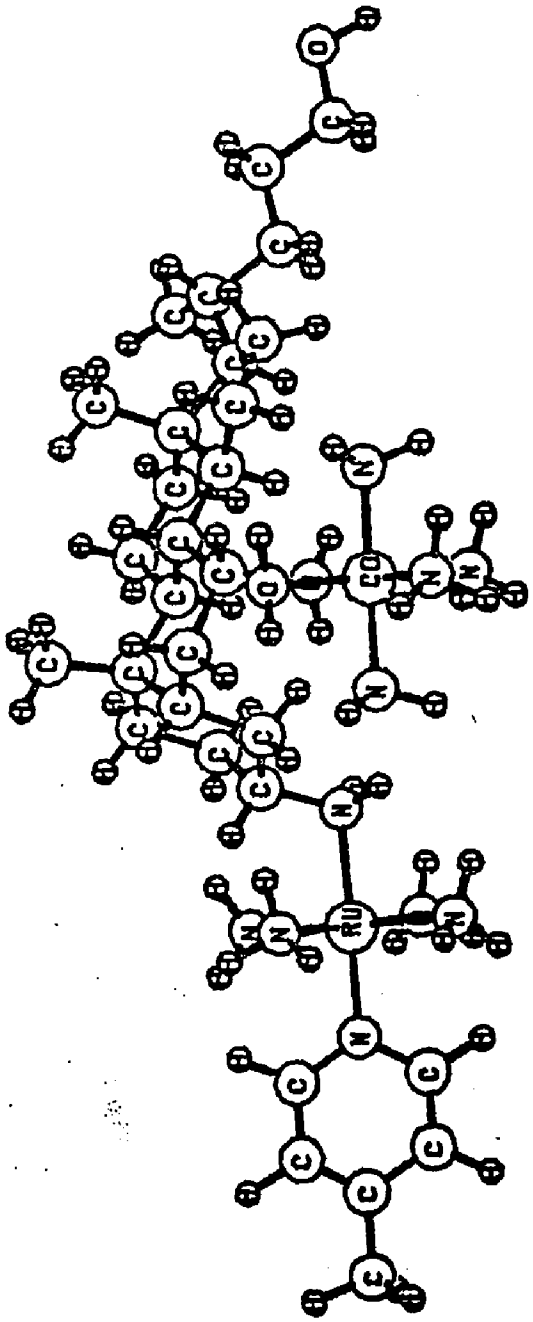

Figure 20. Space-filling Representation of $[(pic)(NH_3)_4Ru(3,7dac)Co(NH_3)_4(H_2O)]^{5+}$.

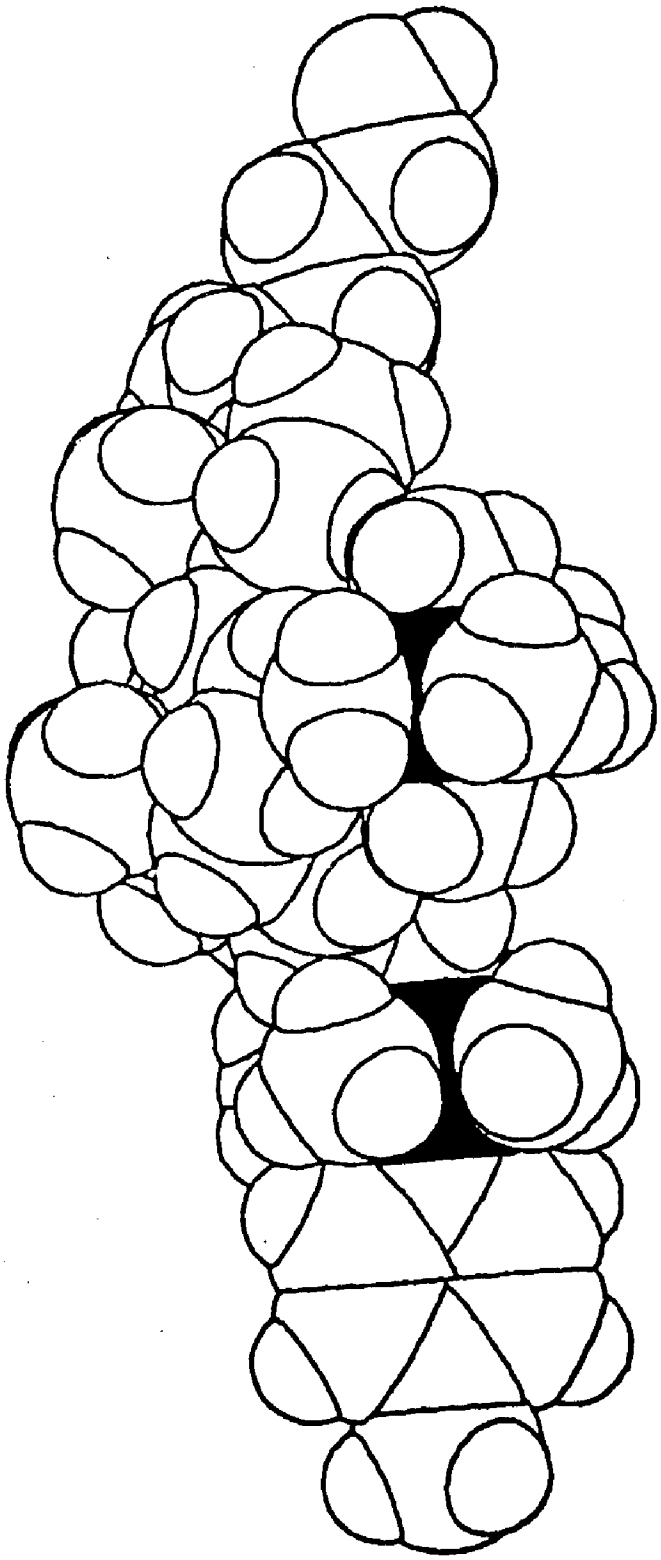

$N_3(\alpha),N_{17}(\beta)$, 4% $N_3(\beta),N_{17}(\alpha)$, and 1% $N_3(\alpha),N_{17}(\alpha)$.

Proton NMR spectroscopy give further evidence that the major product is $N_3(\beta),N_{17}(\beta)$. The chemical shift of the sharp $CH_3(18)$ signal is at 0.62 ppm, matching closely a signal observed for 17β-amino-5α-androstane at 0.61 ppm. The 17α-amino isomer shows this $CH_3(18)$ signal at 0.66 ppm, (see Figure 21 for the NMR spectrum of 3β,17β-diamino-5α-androstane). The peak at 0.81 ppm is assigned to $CH_3(19)$, matching the same shift reported for the 17-amino-5α-androstanes. The region of methine peaks more closely resembles the $N_3(\beta)$ assignment than the $N_3(\alpha)$ assignment. For 3β-amino-5α-androstane, the methine region is from 2.3 to 2.8 ppm, whereas for the 3α-amino-5α-androstane the resonances are observed to be sharper and fall between 3.1 to 3.4 ppm. The methine region for the 3,17-diamino-androstane is rather broad and lies between 2.3 and 3.3 ppm. The center of the methine resonances is found at 2.9 ppm in closer agreement with the spectrum of the $N_3(\beta)$ isomer.

Based on above considerations, the 3β,17β-diamine-5α-androstane was chosen for distance analysis using the Prophet system. The crystallographic coordinates for 3β,17β-dihydroxy-5α-androstane were obtained from the Public Molecules Table of Crystallographic Coordinates. These coordinates were used to obtain structural parameters for the diamino-derivative. Standard N-C bond lengths as well as the dihedral angles calculated for the hydroxyl analog were used. The metal complex fragments were attached in the same manner as for the 3,7dac structural model. Optimized dihedral angles were found for both metal centers by the same cryteria used for the 3,7dac case. The distance calculated between metal centers is 13.36 Å. Figure 22 shows the ORTEP drawing, and Figure 23 the space-filling representation for this molecule.

Figure 21. Proton NMR Spectrum of 3β,17β-diamino-5α-androstane.

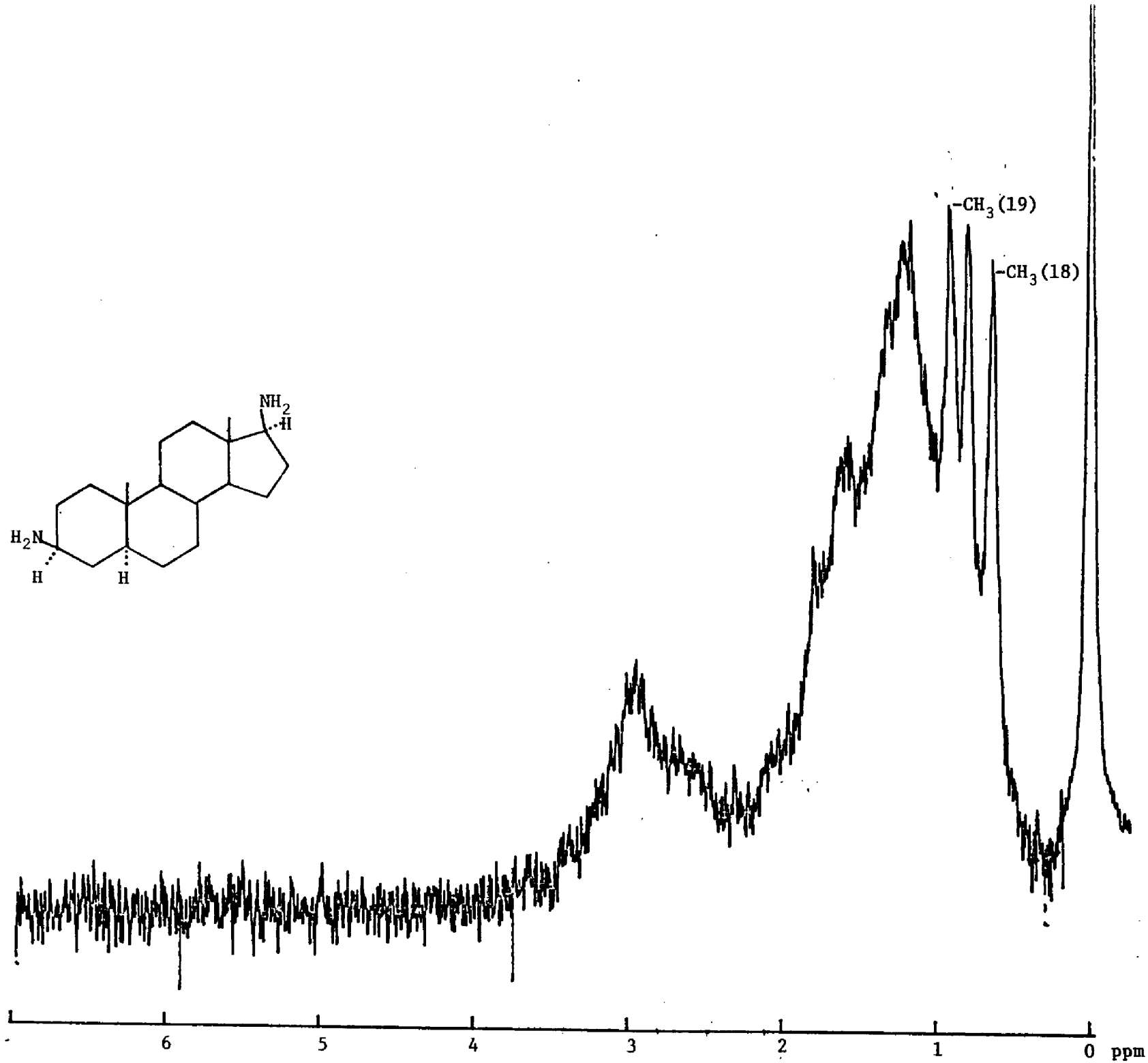
-CH3 (19)
-CH3 (18)
NH2
H
H2N
H
H
6
5
4
3
2
1
0
ppm

Figure 22. ORTEP2 Representation of $[(pic)(NH_3)_4Ru(3,17daa)Co(NH_3)_4(H_2O)]^{5+}$.

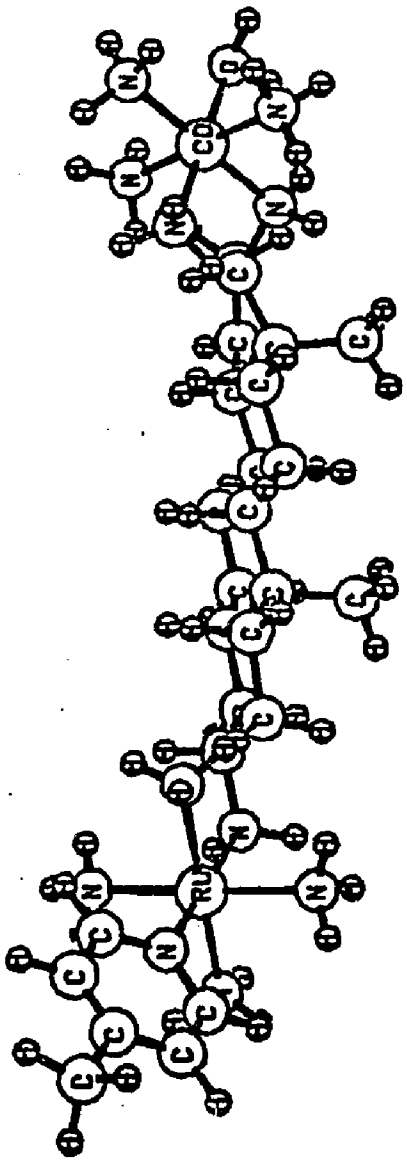

Figure 23. Space-filling Representation of $[(pic)(NH_3)_4Ru(3,17daa)Co(NH_3)_4(H_2O)]^{5+}$.

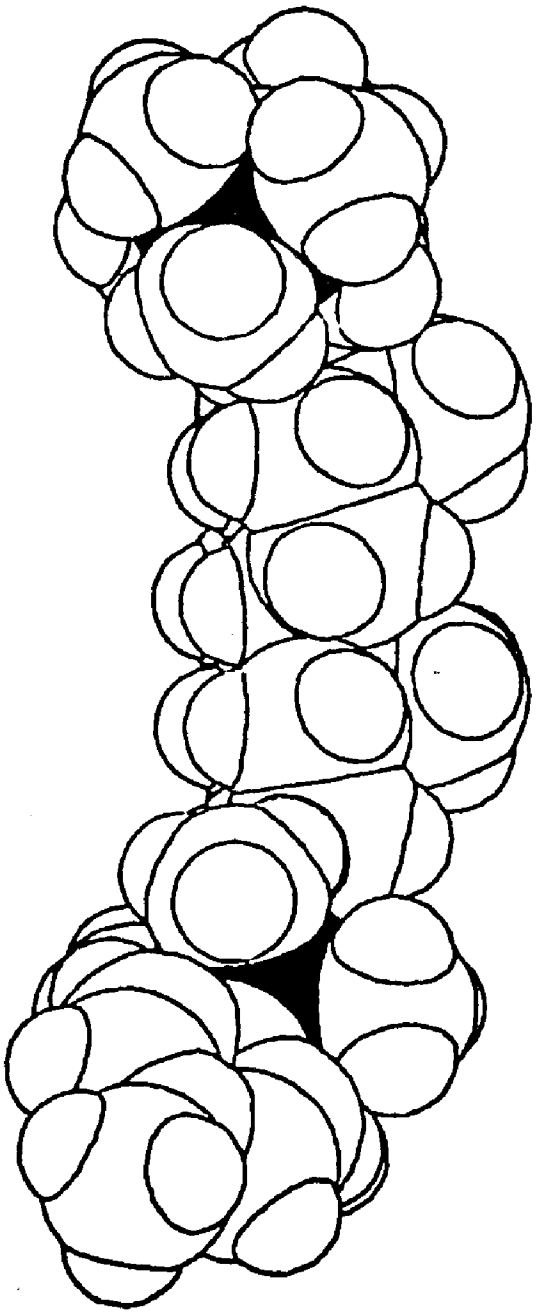

D. Consideration of Bimetallic Complex Reactions

Results of this investigation are summarized in Table XVII. Second order rate constants do not vary over a significant range. Activation parameters of the intermolecular (second order) electron transfers are similar for the two rigid steroid systems. The non-rigid $[(pic)(NH_3)_4Ru$-$(pacm)Co(NH_3)_4(H_2O)]^{5+}$ system has both larger enthalpies and entropies of activation. In all the intermolecular cases studied, a large positive $\Delta S^{\ddagger}$ is observed.

The large positive activation entropies could result from solvent rearrangement in the formation of the activated complex. The approach of one metal site on one molecule to a metal site of another molecule could create a hydrophobic region around the charged centers. In aqueous solution, this could disorganize the water which originally solvated the complex before formation of the activated complex.

The most important consideration with the electron transfer date is the mechanism leading to identical first order rate constants. Various reactions leading to changes in the ruthenium-picoline charge transfer must be considered, since this absorption band was used to follow the kinetic investigation.

E. Mechanisms and Experimental Critique

The following is a discussion of mechanisms leading to the observed changes in the ruthenium-picoline charge transfer band. Each mechanism is compared to the experimental results reported in this thesis. Mechanisms predicted should be consistent with these experimental results: 1) an observable change in the ruthenium-picoline charge transfer; 2) at conditions where $[Ru]_{total} = [Co]_{total}$; 3) with analyzed kinetic experiments where $[Eu^{2+}]_{initial} = [Co^{2+}]_{final}$;

Table XVI. Summary of Electron Transfer Reactions for $[(pic)(NH_3)_4Ru(L)Co(NH_3)_4(H_2O)]^{5+}$.[b]

	Second Order					First Order		
L	k_{et} $M^{-1}s^{-1}$	$\Delta H^{\ddagger}$	$\Delta S^{\ddagger}$	$E_{\frac{1}{2}}$ V	d Å	k_{et} s^{-1}	$\Delta H^{\ddagger}$	$\Delta S^{\ddagger}$
pacm	0.37 [a]	31.4	45.0	0.224	-	-	-	-
3,7dac	4.2	22.7	20.5	0.246	7.47	1.41×10^{-4}	21.0	-5.6
3,17daa	1.9	21.9	16.2	0.238	13.36	1.42×10^{-4}	21.2	-5.0

$\Delta H^{\ddagger}$ is in kcal/mole

$\Delta S^{\ddagger}$ is in cal/mole·°K

[a]Extrapolated from temperature dependence data to 25°C.

[b]All rate constants listed are at 25°C.

4) reactions with only the Ru(II)-L complex, separate or in the presence of Co^{2+} from priviously reduced bimetallic complex, giving different (slower) rate constants than in the presence of Co(III);
5) regeneration of the ruthenium-picoline charge transfer band at 388 nm after the initial reaction has reached completion.

Ruthenium Hydrolysis from the Steroid Complex

There are two types of hydrolyses possible for the ruthenium complexed to the steroid, one is the hydrolysis of the picoline, the other is the hydrolysis of the steroid. Both reactions would result in a change of the charge transfer band. Picoline hydrolysis would have the most dramatic effect as the intense MLCT ($\varepsilon \approx 4 \times 10^3$ liter per mole·cm) would be lost. The product absorption bands should then result from d-d transitions of aquopentaammine ruthenium(II) with $\varepsilon \approx 1 \times 10^2$ liter/mole·cm. Changes in the charge transfer would also be predicted if the steroid was hydrolized from the ruthenium complex. The observed shift would be to the red for ruthenium(II) aquotetraammines.[48]

Any hydrolysis of the ruthenium should lead to a charge transfer change. Direct evidence eliminating this possibility is demonstrated in the regeneration of the charge transfer band at 388 nm. Further contradiction to ruthenium hydrolysis is that a separate reaction is observed when Co(III) is present. It is unlikely that $[Co(NH_3)_5(H_2O)]^{3+}$ would act as a mediator in a substitution reaction since cobalt(III) complexes are substitution inert.

Cobalt Hydrolysis from the Steroid Complex Leading to Electron Transfer

A first order rate would be observed in cobalt hydrolysis if the dissociation from the steroid complex is the rate determining step. A decrease in the ruthenium MLCT would then occur in a faster inter-

molecular electron transfer reaction with the hydrolized cobalt complex. Observed rate constants for pentaammine cobalt hydrolysis (which are for the exchange of the aquo ligand) are very small (about fifty times less than the rates seen for the electron transfers in these binuclear complexes,[56] and even smaller for the loss of amine in $Co(NH_3)_6^{3+}$ by at least five orders of magnitude.[57] Stock solutions for each kinetic series were used for two to three weeks during the course of investigation, over which time the cobalt would have been totally hydrolized if 10^{-4} s^{-1} was the rate constant of cobalt hydrolysis. Under these circumstances, second order behavior would be expected for all concentrations studied since $[Ru]_{total} = [Co]_{total}$. This was not observed.

Direct evidence for cobalt hydrolysis may be obtained experimentally since the cobalt(III) aquotetraammine complex would show a different absorption spectrum (512 nm) from the cobalt(III) diaquotetraammine steroid complex (506 nm). The cobalt(III) diaquotetraamine complex would also have a reduction potential less than a cobalt(III) aquopentaammine complex, which would affect electron transfer rates. Intermolecular reactions of Ru-L-Co could be further probed by studying the reactions of Ru(II)-L with $[Co(NH_3)_5(H_2O)]^{3+}$ and with $[Co(NH_3)_4(H_2O)_2]^{3+}$. Comparison of rates with these cobalt complexes could demonstrate the similarities between the cobalt(III) pentaammine type complexes, as well as support or eliminate the contention of hydrolysis of cobalt as a contributing factor to electron transfer.

Electron Transfers of Ru^{2+} and Co^{3+} on Separate Molecules

Until a good elemental analysis of the bimetallic complexes are obtained, consideration must be given to the possible reaction of ruthenium and cobalt on separate molecules (other then the inter-

molecular reaction of Ru-L-Co). The possible complexes present could be Ru-L, Ru-L-Ru, Co-L, and Co-L-Co. These molecules would be expected to react as separate ions in solution and since $[Ru]_{total} = [Co]_{total}$, a bimolecular rate law should be observed at all concentrations studied. This conclusion is not supported by the system studied in this thesis. In addition, the synthetic design of the metal-steroid complexes utilized an excess of steroid for the reaction with ruthenium. The unreacted steroid should then be easily extracted into chloroform. This extraction precedes the cobalt addition, which would also help eliminate the possibility of cobalt-steroid complexes free of ruthenium. This result still remains to be proven conclusively.

Reactions with Tosylate and/or 4-morpholineethanesulfonic Acid

The ionic strength was controlled in this series of kinetic studies with 0.08 M NapTs and 0.02 M MES. Both of these reagents are at concentrations where pseudo first order kinetics would be observed even with the bimetallic complex concentrations at 2.4×10^{-4} M, which is the largest concentration of bimetallic complex studied in this thesis. The second order behavior observed at 2.4×10^{-4} M would contradict such a mechanism. Supporting evidence against reactions with the counter ion or the buffer is found in the reaction rates being dependent on the presence of Co(III). One method to test such a mechanism is to change the concentration of NapTs and/or the concentration of MES, and to then show the rate change observed is consistent with the postulated pseudo first order mechanism.

Reactions Resulting from Steroid Decomposition

The stability of the steroid during the kinetic investigation may be presumed by chemical intuition. In the synthesis of the

steroid derivatives, strong reductants ($NaBH_3CN$ and sodium metal) were used in forming the amine precursors to the binuclear complexes. In those synthetic reactions, the hydrocarbon backbone remains intact which is evident from the infrared spectra. The mild reductants used in the kinetic investigations (Eu^{2+} and $Ru(NH_3)_6^{2+}$) should therefore not interfere with the integrity of the steroid backbone. Elemental analysis or C^{13} NMR of the products should verify steroid integrity.

Photochemical Reactions

The possibility of photochemical reactions should be considered since ruthenium(II)-pyridine type complexes are known to have photochemical excited states which undergo further chemical reactions.[57] If such a reaction would occur, a shift in the metal to ligand charge transfer band would be expected as the absorption of the MLCT is sensitive to substitution on the pyridine ring.[47] By adding Eu^{2+} to the previously reacted Ru-L-Co complex, the MLCT band is regenerated at 388 nm. This observation would be unlikely had the picoline reacted by a photochemical pathway. Furthermore, the presence of Co(III) would not be expected to influence such a photochemical process, which again is in contradiction to the system investigated in this thesis.

Dimerization of Binuclear Complexes

Stacking, or dimerization, of the binuclear complex in a fast step followed by an electron transfer would elicit a conversion from second order to first order, which supports the kinetic behavior of the experimental system. The dimer at high concentrations would then transfer electrons between other dimers as an interdimer, second order mechanism. As the dilution continues, electron transfer could occur within the dimer giving a first order, intradimer electron transfer

mechanism. Electrostatic repulson of adjacent metal atoms of like charge could compete with the hydrophobic interaction gained from ligand stacking, however, experimental results agree with this mechanism. An important experiment to test this mechanism would be the addition of excess steroid at low complex concentration. This should break any dimer-complex formation favoring interdimer electron transfer.

Catalytic Reaction

There is the possibility of a catalytic reaction requiring the presence of Co(III) shown below as:

$$(pic)Ru(II)\text{-}L\text{-}Co(III) + X \xrightarrow{slow} (pic)Ru(II)\text{-}L + Co(II) + X^{+} \quad (41)$$

$$X^{+} + (pic)Ru(II)\text{-}L \xrightarrow{fast} (pic)Ru(III)\text{-}L + X \quad (42)$$

This mechanism is consistent with the experimentally observed case where $[Eu^{2+}]_{initial} = [Co^{2+}]_{final}$ upon completion of a kinetic run. This would also explain the conversion of a second order reaction (which would be the intermolecular reaction between Ru-L-Co) to a first order reaction (where the rate of catalysis becomes competitive to the bimolecular electron transfer).

The identity of the impurity, X, may result from mercurous ion, transferred with Eu^{2+} addition to the kinetic system, or from the stainless steel needle used for the injection of the reductant into the cell. Possible impurities such as Fe^{2+}, Cr^{2+}, or Ni^{2+} could result. Reproducibility seen in the kinetic studies reported in this thesis would not be expected with these kind of impurities. The dilution series investigated from 7.1×10^{-5} M to 1.1×10^{-5} M for 3,7dac-bimetallic complex and from 6.8×10^{-5} M to 2.4×10^{-5} M for the 3,17daa-bimetallic complex required the volumes of the cells to be varied over a 12 ml range while the volume of Eu^{2+} remained essentially constant at

.12 ml. It is rather unlikely that these rates would be so reproducible since the rates of these reactions would be dependent on the amount of X present. Two experiments may be run to thoroughly disprove these types of contaminants. One way would be to generate Eu^{2+} by coulometric methods, thereby eliminating mercurous ion contamination. The other way would be to use platinum needles which do not corrode as easily as stainless steel.

Intramolecular Electron Transfer

Support for intramolecular electron transfer as the first order path is in the kinetic behavior of the system. The dependence of rate on concentration changes from second order to first order as would be predicted upon going from an intermolecular to an intramolecular mechanism. The enthalpies of activation remain consistent in the conversion from second order to first order (22 kcal/mole) suggesting the same electron exchange reaction with internal bond adjustments of the inner coordination sphere providing most of the activation barrier in the two pathways. These enthalpies of activation are also very similar to the series studied by Zawacky for electron transfer in Ru-nicotinate-Co derivatives.[58]

All other experimental observables are consistent with this mechanism. The only contradiction to the considerations presented in this thesis involves any distance dependence for electron transfer. There is no difference in rate of reaction between the bimetallic-3,7dac complex where the separation destance between redox centers is 7.47 Å, and the bimetallic-3,17daa where this distance is 13.36 Å. To see if such a contradiction is warranted, a Marcus theory calculation of the predicted free energy of activation is examined.

F. Marcus Theory Calculations of Free Energies of Activation

The experimentally observed free energies of activation for reactions of the steroid complexes were compared to free energies of activation calculated by Marcus theory.[59] For calculating the contribution to the free energy of activation due to inner-sphere reorganization, $\Delta G^{\ddagger}_{in}$, the value used by Sutin for Ru(II) in his treatment of the $Ru(NH_3)_5pz^{2+/3+}$ self exchange reaction of 1.0 kcal/mole was chosen.

The classical calculation for $\Delta G^{\ddagger}_{in}$ using only ground state vibrations (Stynes and Ibers),[41] gives 6.8 kcal/mole for $Co^{III/II}$, but this does not account for spin multiplicity effects. The spin changes which occur when Co(III) (high spin) is reduced to Co(II) (low spin) affects the Franck-Condon factor between vibrational states at the intersection of the potential energy curves (this factor is presumed to be about one for the calculation by Stynes and Ibers) as well as reducing the probability of reaction due to the spin restriction itself. Calculations involving thermally excited electronic states lead, however, to estimates of $\Delta G^{\ddagger}_{in}$ for the $Co^{III/II}$ reaction which are much higher than observed values for the total free energy of activation.

Buhks, et al.[56] have calculated the difference in $\Delta G^{\ddagger}_{in}$ for $Co^{III/II}$ vs $Ru^{II/III}$ using a quantum mechanical approach. The spin multiplicity effects are calculated to be 5.5 kcal/mole while the thermal average of Franck-Condon factors between excited vibrational states is 11.1 kcal per mole. The total for the $Co^{III/II}$ contribution to $\Delta G^{\ddagger}_{in}$ should then be 16.6 kcal/mole. Since $\Delta G^{\ddagger}_{in}$ calculated for $Ru^{II/III}$ is 1.0 kcal/mole the estimate for the contribution to the total free energy of activation should be 17.6 kcal/mole. The range of reliability for these calcula-

lations is estimated to be from about 19 to 14 kcal/mole ($k_{Co}/k_{Ru} \simeq 10^{-12\pm2}$). Equations 4, 6, and 7 were used for the free energy of activation calculations ($\Delta G^{\ddagger}_{trans}$ and w_r are assumed to be negligible). The results of these calculations are shown in Table XVII.

The contribution of $\Delta G^{\ddagger}_{out}$ to the total $\Delta G^{\ddagger}$ is less than the $\Delta G^{\ddagger}_{in}$ for these complexes. The difference between $\Delta G^{\ddagger}_{out}$ for the 3,7dac-binuclear complex and the 3,17daa-binuclear complex is 2.6 kcal/mole. With this small difference, calculations still suggest the ratio of rates between the two steroid-complexes should be around 75. It would be truly startling if Marcus theory can be applied to systems in which the coordination spheres are separated by 6 Å. Marcus theory is only applicable when the coupling between the reactant wave functions is relatively large (≈0.5 kcal/mole) which have always been assumed to require contact of the first coordination sphere.

A more noticeable effect in the ratio of rates for the two steroid complexes would have been expected if electron transfer goes through the nonadiabatic route predicted by Hopfield theory. The results reported here comply more favorably with outer-sphere electron transfer, even with a distance of 6.0 Å separating the inner coordination spheres of the redox centers, if indeed the first order kinetics observed are the intramolecular electron transfer reactions.

G. Summary of Results

In considering several possible mechanisms, conversion from second order to first order kinetics could result from the conversion of an intermolecular electron transfer mechanism to some other, rate limiting first order mechanism. Such mechanisms have been considered in the previous section, however, contradictions do exist with most of these

Table XVII. Comparison of Observed and Calculated Free Energies of Activation for First Order Electron Transfer at 25°C.[a]

	3,7dac	3,17daa
$k\ s^{-1}$	1.4×10^{-4}	1.4×10^{-4}
d Å	7.5[b]	13.4[b]
$\Delta G^{\ddagger}_{out}$	6.3	8.9
$\Delta G^{\ddagger}_{in}$	17.6[c]	17.6[c]
$\Delta G_o/2$	-1.1[d]	-1.1[d]
$\Delta G^{\ddagger}_{calc}$	22.8	24.4
$\Delta G^{\ddagger}_{obs}$	22.7	22.7

[a]Dimensions for $\Delta G^{\ddagger}$ are in kcal/mole.

[b]Based on distances calculated from the Prophet constructed molecules.

[c]See text for discussion of $\Delta G^{\ddagger}_{in}$.

[d]Calculated from electrochemical data and from the value predicted for the reduction potential of the aquopentaammine cobalt complex.[60]

considerations. Two mechanisms consistent with the experimental results including the conversion from second order to first order kinetics are dimerization and intramolecular electron transfer. Consideration of Marcus theory on the prediction of free energies of activation for both steroid complexes actually supports the observed rate constants, rather than contradict them. Until the composition of the complexes being studied may be clearly identified, however, a firm conclusion may not be reached.

Elemental analysis of bimetallic complexes show an excess of Cl^- at nearly 20% of the value calculated for the complex analyzed. This chloride impurity most likely results from the chloride anion exchange column whcih is used just before the bimetallic complex is collected. Attempts to recrystallize these complexes failed. Recrystallization in concentrated acid resulted in hydrolysis of the ruthenium complex. Recrystallization using saturated salt solutions resulted in a large excess of salt in the product. Most likely a solvent system will be chosen to recrystallize these products. The chloride salt is slightly soluble in ethanol. Perhaps various proportions of water/ethanol solutions may be used to collect these products.

Another method for structural analysis could be C^{13} NMR spectroscopy, comparing chemical shifts for free ligands with those for metal complexes. A suggested experiment is to record spectra of the Ru(III)-L-Co(III) complex since cobalt(III) is diamagnetic and Ru(III) generally leads to readily observed shifts and not too much line broadening.

H. Concluding Remarks

The range of distances involved in cytochrome electron transfer may be limited in scope. Such a conclusion is supported by data gathered from crystal structures and computer simulations. More recently, information has been supplied through the use of inorganic kinetic probes which give reasonable values of site-to-surface protein distances.[61] This range of prosthetic group separations seems likely to be limited to about 8 Å. Values calculated for site-to-surface distances by Gray for cytochrome c is 3.4 Å and cytochrome c_{551} as 4.0 Å. Combining this information with the computer simulation data of Salemme,[1] gives the site-to-surface value for cytochrome b_5 of 4.0 Å. Gray calculates a site-to-surface value for HIPIP as 5.8 Å, and perhaps the cytochrome interacting with HIPIP could give a site-to-surface value of 2.5 Å (2.6 Å is the site-to-surface value calculated by Gray for plastocyanin, a blue copper protein). The true exception to this small range in separation could be the oxidases or peroxidases, which may undergo electron transfer by a completely different mechanism.

A rather thorough structural study was recently reported by Kraut for cytochrome c-cytochrome peroxidase where the prosthetic groups are separated by 16.5 Å.[8] For electron transfers over these distances, a low lying "supramolecular" conduction orbital (organic semiconduction) is proposed. Structural features support this postulation. The two heme groups are nearly perfectly parallel, and the molecular interface consists of aromatic, conjugated groups whose planes are parallel to the common heme-heme plane.

Since the peroxidase and the a_3 site in cytochrome oxidase involve oxygen chemistry, they may not be as efficient as the coordinatively

fixed cytochromes at transferring electrons, and π aromatic orbitals may be utilized to supply their electron requirement. For these reasons, the oxidases and peroxidases may be exceptions to the range limit of the other cytochromes.

The range limit between prosthetic groups may also be the answer to the selective, stepwise transfer of electrons down a particular metabolic pathway. Kraut also postulates a "plug in socket" rationale which he again demonstrated in his cytochrome c-cytochrome peroxidase system (which transfers electrons rather efficiently at 10^8 $M^{-1}s^{-1}$). Similar plug in socket mechanisms could apply to other cytochrome surfaces. In such cases the contact is made at specific interacting surface sites and the distance requirements are thus met for outer-sphere electron transfer.

Further support for outer-sphere electron transfer lies within the structure of the prosthetic groups. In the iron-sulfur clusters, bond adjustments are minimized between the Fe(II) and Fe(III) states.[62] Heme containing cytochromes have axial ligands fixing the iron centers into the low spin state, also minimizing the bond adjustment between Fe(II) and Fe(III). For the copper containing cytochromes, experimental evidence supports a geometry between square planer and tetrahedral, which would minimize the bond adjustment between Cu(I) and Cu(II).[63] By minimizing bond adjustments, inner-sphere reorganization energies are minimized, greatly reducing the total activation energy for outer-sphere electron transfer.

If the outer-sphere mechanism does account for electron transfer a 6 Å separation between redox coordination spheres, as with the 3,17daa-binuclear complex, why not 7 Å, or 8 Å? What is the limit to the

"reach" of outer-sphere reactions? Continued studies with similar systems to those presented in this thesis are being prepared to help answer these questions.

REFRENCES

(1) Salemme, F.R. "Tunneling in Biological Systems", Chance, B., DeVault, D.C., Frauenfelder, H., Marcus, R.A., Schrieffer, J.R., Sutin, N., Eds.; Academic Press: New York, (1979); p 525.

(2) Marcus, R.A. Discussions Faraday Soc. (1960), 29, 21.

(3) Hopfield, J.J. Proc. Nat. Acad. Sci. USA (1974), 71, 3640.

(4) Chien, J.C.W. J. of Phys. Chem. (1978), 82, 2158.

(5) Vanderkooi, J.; Ercinska, M. Eur. J. of Biochem. (1975), 60, 199.

(6) Vanderkooi, J.; Leigh, J.S.; Owen, C.S.; Glatz, P.; Blum, M. "Frontiers of Biological Energetics", Vol 1, Academic Press: New York, (1978); p 54.

(7) Erecinska, M. "Tunneling in Biological Systems", Chance, B., DeVault, D.C., Frauenfelder, H., Marcus, R.A, Schrieffer, J.R., Sutin, N., Eds.; Academic Press: New York, (1979); p453.

(8) Kraut, J. Biochem. Soc. Trans. (1981), 197.

(9) Bennet, "Tunneling in Biological Systems", Chance, B., DeVault, D.C., Frauenfelder, H., Marcus, R.A., Schrieffer, J.R., Sutin, N., Eds.; Academic Press: New York, (1979); p 543.

(10) Jortner, J. J. Chem. Phys. (1976), 64, 4860.

(11) Wilkins, R.G. "The Study of Kinetics and Mechanism of Reactions and Transition Metal Complexes", Allyn and Bacon: Boston, (1974).

(12) Basolo, F. Pearson, R.G. "Mechanisms of Inorganic Reactions", 2nd Ed., John Wiley and Sons: New York, (1967).

(13) Miller, J.R. "Tunneling in Biological Systems", Chance, B., DeVault, D.C., Frauenfelder, H., Marcus, R.A., Schrieffer, J.R., Sutin, N., Eds.; Academic Press: New York, (1979); p 95.

(14) Ford-Smith, M.H.; Sutin, N. J. Am. Chem. Soc. (1961), 83, 1830.

(15) Dutz, G.; Sutin, N. Inorg. Chem. (1963), 2, 917.

(16) Sutin, N. "Tunneling in Biological Systems", Chance, B., DeVault, D.C., Frauenfelder, H., Marcus, R.A., Schrieffer, J.R., Sutin, N., Eds.; Academic Press: New York, (1979); p 204.

(17) Forster, T. Naturwissenschaften (1946), 33, 166.

(18) Dexter, D.L. J. Chem. Phys. (1953), 21, 831.

(19) DeVault D.; Chance, B. Biophys. J. (1966), 6, 825.

(20) Devault, D.; Parkes, J.H.; Chance, B. Nature (London) (1966), 215 642.

(21) Dutton, P.L. Biochem. Biophys. Acta (1971), 226, 63.

(22) Chien, J.C.W.; Gibson, H.L.; Dickenson, L.C. Biochemistry (1978), 17, 2579.

(23) Miralles, A.J.; Armstrong, R.F.; Haim, A.J. J. Am. Chem. Soc. (1977), 99, 1416.

(24) Balzani V.; Scandola, T.; Orland, B.; Sabbatini, N.; Indelli, M.T. J. Am. Chem. Soc. (1981), 103, 3370.

(25) Endicot, J.F.; Taube, H. J. Am. Chem. Soc. (1964), 86, 1686.

(26) Isied, S.S.; Taube, H. J. Am. Chem. Soc. (1973), 95, 8198.

(27) Glick, V.P.; Schmonsees, W.G.; Endicott, J.F. J. Am. Chem. Soc. (1974), 96, 5661.

(28) Endicott, J.; Lillie, J.; Koszaj, J.M.; Ramaswamy, B.S.; Schomsees, W.G.; Simic V.G.; Glick, M.P.; Rillema, D.P. J. Am. Chem. Soc. (1977), 99, 429.

(29) Job, R.C. Personal Comments.

(30) Lavallee, C. Ph.D. Thesis, University of Chicago, (1978).

(31) O'Halloran T.V.; Malin, J.M. personal Comments.

(32) Kauffman, G.B.; Pinnell, R.P. "Inorganic Synthesis", Volume 6, Rochow, E.G., Ed.; RcGraw-Hill: New York, (1960); p 176.

(33) Dixon, N.E.; Jackson, W.G.; Lancaster, M.J.; Lawrance, G.A.; Sargeson, A.M. Inorg. Chem. (1981), 20, 470.

(34) Vogt, L.H.; Katz, J.L.; Wiberley, S.E. Inorg. Chem. (1965), 4, 1157.

(35) Marchant, J.A.; Matsubara, T.; Ford, P.C. Inorg. Chem. (1977), 16, 2160.

(36) Diamond, S.E.; Tom, G.M.; Taube, H. J. Am. Chem. Soc. (1975), 97, 2661.

(37) Leal, O.; Anderson, D.L.; Bowman, F.G.; Basolo, F.; Burwell, R.L. Jr. J. Am. Chem. Soc. (1975), 97, 5125.

(38) Rindone, W.P.; Kush, T. Eds. "Prophet Molecules", Bolt Beranek and Newman Inc.: Cambridge, Mass., (1980).

(39) Batta, A.K.; Salen, G.; Blount, J.F.; Shefer, S. J. of Lipid Res. (1979), 20, 935.

(40) Rindone W.P.; Kush, T. "Prophet Molecules", Bolt Beranek and Newman Inc.: Cambridge, Mass., (1980); B-1.

(41) Stynes, H.C.; Ibers, J.A. Inorg. Chem. (1971), 10, 2304.

(42) Gress, M.E.; Creutz, C.; Quicksall, C.O. Inorg. Chem. (1981), 20, 1522.

(43) Kirkland, J. Anal. Chem. (1955), 27, 1537.

(44) Matsubara, T.; Ford, P. Inorg. Chem. (1976), 15, 1107.

(45) Chen, M.; Creutz, C.; Sutin, N. J. Am. Chem. Soc. (1977), 99, 5615.

(46) Lilie, J.; Shinogara, B.; Simia, M.G. J. Am. Chem. Soc. (1976), 98; 6516.

(47) Ford, P.; Rudd, D.F.P.; Gaunder, R.; Taube, H. J. Am. Chem. Soc. (1968), 90, 1187.

(48) Isied, S.S.; Taube, H. Inorg. Chem. (1976), 15, 3070.

(49) Tfouni, E.; Ford, P. Inorg. Chem. (1980), 19, 72.

(50) Evans, I.P.; Everett, B.W.; Sargeson, A.M. J.C.S. Chem. Comm. (1975), 140.

(51) Guengerich, C.P.; Schug, K. J. Am. Chem. Soc. (1977), 99, 3298.

(52) S. Jeganathan, Personal Comments.

(53) Bhattacharyya, D.K.; Bankawala, Y.G. Anal. Chem. (1978), 50, 1462.

(54) Cowell, D.B.; Davis, A.K.; Mathieson, D.W.; Nicklin, P.D. J. Chem. Soc. Perkin Trans. I (1974) 1505.

(55) Hunt, H.R.; Taube, H. J. Am. Chem. Soc. (1958), 80, 2642.

(56) Buhks, E.; Bixon, M.; Jortner, J.; Navon, G. Inorg. Chem. (1979), 18, 2014.

(57) Hintze, R.E.; Ford, P.C. Inorg. Chem. (1975), 14, 1211.

(58) Zawacky, S.K. Ph.D. Thesis, Stanford University, (1979).

(59) Brown, G.M.; Sutin, N. J. Am. Chem. Soc. (1979), 101, 883.

(60) Yalman, R.G. Inorg. Chem. (1962), 1, 16.

(61) Mauk, A.G.; Scott, R.A.; Gray, H.B. J. Am. Chem. Soc. (1980), 102, 4360.

(62) Que, L.; Bobrik, M.A.; Ibers, J.A.; Holm, R.H. J. Am. Chem. Soc. (1974), 96, 4168.

(63) Thompson, J.S.; Marks, I.J.; Ibers, J.A. Proc. Natl. Acad. Sci. U.S.A. (1977), 74, 3114.